PERGAMON

International Journal of Multiphase Flow 27 (2001) 347–378

International Journal of Multiphase Flow

www.elsevier.com/locate/ijmulflow

Statistics in particle-laden plane strain turbulence by direct numerical simulation

C. Barré[a], F. Mashayek[b,*], D.B. Taulbee[a]

[a] *Department of Mechanical and Aerospace Engineering, State University of New York at Buffalo, Buffalo, NY 14260-4400 USA*

[b] *Department of Mechanical Engineering, University of Hawaii at Manoa, 2540 Dole Street, Honolulu, HI 96822 USA*

Received 5 August 1999; received in revised form 6 March 2000

Abstract

Direct numerical simulation is utilized to generate statistics in particle-laden homogeneous plane strain turbulent flows. Assuming that the two-phase flow is dilute (one-way coupling), a variety of cases are considered to investigate the effects of the particle time constant. The carrier phase is incompressible and is treated in the Eulerian frame whereas the particles are tracked individually in a Lagrangian frame. For small particle Reynolds numbers, an analytical expression for the particle mean velocity is found, which is different from the fluid one, and the dispersed phase is shown to be homogeneous. This is not the case for particles with large Reynolds numbers and no statistics involving particle fluctuating velocity is presented for large particles. The results show that the root mean square (r.m.s.) of the particle velocity in the squeezed direction exceeds that of the fluid in the same direction and increases with the particle time constant. The mean velocity gradient component in the elongated direction has the opposite effect, that is the r.m.s. of the particle velocity is decreased below that of the fluid in this direction. Further, the dispersed phase exhibits a larger anisotropy than the fluid phase, and its anisotropy increases with the particle inertia. Dispersion is shown to depend strongly on the injection location and quantified dispersion results show that increasing the injection location coordinates in the strained directions increases the dispersion.

Keywords: Two-phase; Turbulence; Plane strain flow; Direct numerical simulation; Statistics

* Corresponding author. Tel.: +1-808-956-9693; fax: +1-808-956-2373.
E-mail address: mashaye@wiliki.eng.hawaii.edu (F. Mashayek).

0301-9322/01/$ - see front matter
PII: S0301-9322(00)00019-7

1. Introduction

Analytical treatment of two-phase turbulent flows has received a great deal of attention in recent years, due mainly to extensive technological applications (Faeth, 1987; Crowe et al., 1996). With the increase of interest in mathematical modeling of these flows, however, there has been associated a growing demand for experimental and numerical studies that could lead to a more profound physical understanding, in addition to a reliable data bank for model validation. It is now widely accepted that the performance of turbulence models must be assessed in various simple flow configurations before they can be applied to complex flows for which the experimental data are very scarce, if not impossible. During the past two decades direct numerical simulation (DNS) has emerged as a viable means for generating accurate and detail information in turbulent flows with simple geometries. In our previous works (see e.g. Mashayek et al., 1997, 1998; Mashayek, 1998) we have utilized DNS for the investigation of particle-laden isotropic and homogeneous shear turbulent flows. Our experience in implementing the DNS results for both development and assessment of turbulence models has also been very encouraging (Mashayek et al., 1998; Mashayek, 1999). In the present work we apply DNS to another mode of distortion, i.e. the irrotational plane strain flow.

Direct numerical simulation of particle-laden turbulent flows has been pioneered by Riley and Patterson (1974) and then followed by many others (see e.g. McLaughlin, 1989; Wang and Maxey, 1993; Brooke et al., 1994; Pan and Banerjee, 1996; Ling et al., 1998; Miller and Bellan, 1999). Although none of the previous studies have considered the two-phase plane strain turbulent flow, the single-phase plane strain flow has been studied somewhat in detail; an extensive review is not intended here, instead we refer to Lee and Reynolds (1985). Numerical simulations of plane strain flows are performed by Kwak et al. (1975) using large eddy simulations (LES), and by Rogallo and Moin (1984) using DNS. Lee and Reynolds (1985) perform DNS to study the structure of homogeneous turbulence subject to irrotational strains and relaxation. They consider plane strain, axisymmetric contraction and expansion, and secondary plane strain after the axisymmetric strains, and find that in a distorting turbulent flow the turbulence field continuously evolves toward an asymptotic state which is mainly determined by the strain rate imposed during distortion. The turbulent vorticity field is found to be essential for the anisotropy in the turbulent velocity field. For turbulent flows relaxing from strains, they show that the small-scale anisotropies relax rapidly at first and then step with the large-scale anisotropy (locking of relaxation rate). The study by Lee and Reynolds (1985) constitutes the basis for the simulation of the carrier phase in the present study.

While the physical understanding of particle-laden plane strain turbulent flows is the main objective of this work, issues pertaining to modeling of two-phase flows are also considered. To that end, DNS results are utilized to produce statistics which may later be implemented for model validations. Due to the anisotropy of the flow, these statistics could be very valuable for verifying recent models which take the effects of anisotropy into accounts (see e.g. Zhou, 1993; Mashayek et al., 1998). Plane strain is a simple fundamental flow and is a direct model for flow along a stagnation streamline, flow through a contraction, etc., and is an approximate model for irrotational flows in general. Due to these features, plane strain has been, traditionally, one of the flows extensively utilized for model validation in the context of single-phase turbulent flows. In the case of two-phase flows, another feature which distinguishes plane

strain from other geometries currently feasible by DNS, is the presence of a mean velocity difference between the two phases. This allows us to investigate the effects of 'crossing trajectories' while the homogeneity of the flow can be used to calculate accurate statistics using samples from the 'entire' solution domain. Therefore, by considering plane strain turbulent flows, not only one can investigate the effects of the mean velocity gradients, similar to those observed in turbulent shear flows (Liljegren, 1993; Wen et al., 1992; Simonin et al., 1995; Taulbee et al., 1999), but also the effects of a slip velocity between the particle and its surrounding fluid may be studied. The latter effects can be compared to the effects of gravity in isotropic turbulent flows (Maxey, 1987; Wang and Maxey, 1993), which involve the crossing-trajectories effect (Yudine, 1959) and the associated 'continuity effect' (Csanady, 1963). Finally, due to the presence of a mean velocity difference between the phases, plane strain flow can be used to demonstrate the compressibility of the dispersed phase, a feature again not present in the DNS of homogeneous shear flow. In Sections 2 and 3 the formulation of the carrier and the dispersed phases is described, followed by an overview of the numerical simulations in Section 4. The results of the simulations are presented and discussed in Section 5. A summary and some concluding remarks are provided in Section 6.

2. Description of the carrier phase

This work deals with the dispersion of solid particles in a homogeneous plane strain turbulent flow. It is assumed that the two-phase flow is dilute, thus the effects of the particles on the carrier phase are neglected (i.e. one-way-coupling). The carrier phase is incompressible and is treated in the Eulerian frame whereas the particles are tracked in a Lagrangian manner. The continuous carrier phase is assumed to be a Newtonian fluid with constant density (ρ_f) and viscosity (μ). With the assumption of one-way coupling, the transport of the carrier phase is not influenced by the presence of the particles, and is described via the Eulerian continuity and momentum equations:

$$\frac{\partial \hat{U}_j}{\partial x_j} = 0, \quad \frac{\partial \hat{U}_i}{\partial t} + \frac{\partial}{\partial x_j}\left(\hat{U}_i \hat{U}_j\right) = -\frac{\partial \hat{P}}{\partial x_i} + \frac{1}{Re_0}\frac{\partial^2 \hat{U}_i}{\partial x_j \partial x_j}, \tag{2.1}$$

where $\hat{}$ denotes the instantaneous variable, x_i and t are the spatial and temporal coordinates, respectively, and $\hat{U}_i$ and $\hat{P}$ indicate the fluid instantaneous velocity and pressure, respectively. All the variables are normalized by the reference length (L_0), density (ρ_0), and velocity (U_0) scales. The length scale is conveniently chosen such that the normalized volume of the simulation box is $(2\pi)^3$, and the fluid density is used as the scale for density. The velocity scale is found from the box Reynolds number, $Re_0 = \rho_0 U_0 L_0/\mu$ (determination of Re_0 is explained in Section 4).

To configure the plane strain flow, the carrier phase is subjected to a uniform mean strain in two directions such that: $\hat{U}_i = Sx_1\delta_{i1} - Sx_2\delta_{i2} + u_i$, where δ_{ij} is the Kronecker delta function and u_i is the carrier phase fluctuating velocity. The magnitude of the imposed strain is given by $S = \partial U_1/\partial x_1 = -\partial U_2/\partial x_2 = \text{constant}$, where $U_i = \langle \hat{U}_i \rangle$ denotes the Eulerian ensemble-mean (denoted by $\langle\ \rangle$) velocity. The geometry (Fig. 1) is defined by the Cartesian coordinates x_1 (stretched

direction), x_2 (squeezed direction), and x_3 (invariant direction). With this mean velocity gradient, Lee and Reynolds (1985) show that the turbulence is homogeneous. Such flow is, in concept, unbounded, however, in numerical simulations a finite domain may be considered by applying periodic boundary conditions which allows utilization of the Fourier spectral method. This is accomplished by solving the governing equations for fluctuating velocities on a grid which deforms with the mean flow. This transformation has been discussed in detail by Rogallo and Moin (1984) and is only summarized here. A computational (deforming) coordinate system, x_i', is related to the fixed (non-deforming) system through $x_i' = B_{ij}(t)x_j$ where the transformation tensor is defined as:

$$B_{ij}(t) = \begin{pmatrix} B_{11}^0 \exp(-St) & 0 & 0 \\ 0 & B_{22}^0 \exp(St) & 0 \\ 0 & 0 & B_{33}^0 \end{pmatrix}, \qquad B_{ij}(0) = \begin{pmatrix} B_{11}^0 & 0 & 0 \\ 0 & B_{22}^0 & 0 \\ 0 & 0 & B_{33}^0 \end{pmatrix}. \tag{2.2}$$

Applying the transformation, the governing equations for the carrier phase in the deforming coordinate system are expressed as:

$$B_{ji}\frac{\partial u_i}{\partial x_j'} = 0, \quad \frac{\partial u_i}{\partial t'} + U_{i,j}u_j + B_{mj}\frac{\partial (u_i u_j)}{\partial x_m'} + B_{mi}\frac{\partial \mathrm{p}}{\partial x_m'} = \frac{B_{mj}B_{nj}}{Re_0}\frac{\partial^2 u_i}{\partial x_m' \partial x_n'}. \tag{2.3}$$

The computational grid is attached to the deforming frame, and a typical node N is characterized by a triplet of integers (i, j, k) at any time t (Fig. 1). The coordinates of the grid point in the moving system are constant in time, that is:

$$x_1'(t) = x_1'(0) = B_{11}^0 i\Delta, \qquad x_2'(t) = x_2'(0) = B_{22}^0 j\Delta, \quad x_3'(t) = x_3'(0) = B_{33}^0 k\Delta, \tag{2.4}$$

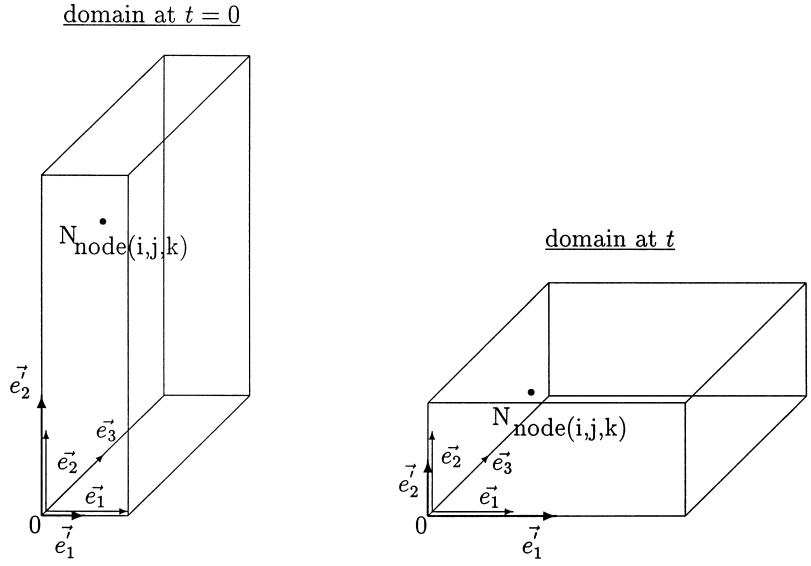

Fig. 1. Computational domain for plane strain flow at times $t = 0$ and t.

where Δ is the grid spacing and is identical for all three directions. This implies that the new vector basis ($\vec{e}_i'$) is a function of time:

$$\vec{e}_1'(t) = \frac{\exp(St)}{B_{11}^0}\vec{e}_1, \qquad \vec{e}_2'(t) = \frac{\exp(-St)}{B_{22}^0}\vec{e}_2, \qquad \vec{e}_3'(t) = \frac{1}{B_{33}^0}\vec{e}_3. \tag{2.5}$$

Therefore, $\vec{e}_i'$ is not a normal basis for the usual norm associated with the inertial frame (see Fig. 1). We note that the x_3-direction is, however, invariant under this transformation ($B_{33}(t) = B_{33}^0 = 1$). There is indeed no mean strain and no mean velocity along this axis, and $x_3'(t) = x_3(t) = x_3(0)$ and $\vec{e}_3'(t) = \vec{e}_3(t) = \vec{e}_3(0)$. It should also be emphasized that by solving Eq. (2.3), we obtain the fluctuating velocity components u_i in the inertial coordinate system. For the purpose of this study, there is no need to solve $u_i' = B_{ij}u_j$ for the velocity vector in the moving frame.

3. Description of the dispersed phase

The solid particles are assumed to be spherical with diameter smaller than the smallest length scale of the turbulence. Since the volume fraction of the dispersed phase is small, the particle–particle collisions can be neglected. The particle density is much larger than the fluid density such that only the drag force and inertia are significant to the particle dynamics. With these assumptions, the Lagrangian equations of motion for the discrete particles reduce to

$$\frac{\mathrm{d}\hat{X}_i}{\mathrm{d}t} = \hat{V}_i, \quad \frac{\mathrm{d}\hat{V}_i}{\mathrm{d}t} = \frac{f}{\tau_p}\left(\hat{U}_i^* - \hat{V}_i\right), \tag{3.1}$$

where $\hat{X}_i$ and $\hat{V}_i$ are the particle instantaneous position and velocity, respectively. The superscript * indicates the fluid variable evaluated at the particle location. The particle time constant for Stokesian drag of a spherical particle is defined as $\tau_\mathrm{p} = Re_0\rho_\mathrm{p}\mathrm{d}_\mathrm{p}^2/18$ where ρ_p and d_p are the nondimensional particle density and diameter, respectively. The particle variables are normalized using the same reference scales as those used for the carrier phase variables. The parameter $f = 1 + 0.15Re_\mathrm{p}^{0.687}$ describes an empirical correction to Stokesian drag for large particle Reynolds numbers ($Re_\mathrm{p} = Re_0\mathrm{d}_\mathrm{p}|\hat{U}_i^* - \hat{V}_i|$) and is valid for $Re_\mathrm{p} < 1000$ (Wallis, 1969).

For the low-volume-fraction and high-density-ratio particle-laden flow considered here, the second of Eq. (3.1) can be also viewed as an Eulerian equation for the velocity of the dispersed phase, derived via either volume averaging (Jackson, 1997) or ensemble averaging (Zhang and Prosperetti, 1997). Then, the velocity determined at each point in space from the Eulerian equation can also represent the Lagrangian velocity of a particle whose trajectory passes through the same point at the same instant in time. In the following we use the Eulerian representation to discuss the conditions required for homogeneity of the dispersed phase. The relations governing the mean velocity of the particles are derived using the Lagrangian equations.

We have seen that the carrier phase is homogeneous and that provided a linear transformation, periodic boundary conditions can be applied to the turbulent plane strain flow. The extension of this transformation to the dispersed phase, however, is not straightforward as

the particles do not have the same mean velocity as that of the carrier phase. To make this point clear, we consider the mean particle momentum equation derived by ensemble averaging of the Eulerian form of (3.1):

$$\frac{D^V V_i}{Dt} = \ll \frac{f}{\tau_p}\left(\hat{U}_i^* - \hat{V}_i\right) \gg - \ll v_j \frac{\partial v_i}{\partial x_j} \gg . \tag{3.2}$$

Here $\frac{D^V}{Dt} = \frac{\partial}{\partial t} + V_j \frac{\partial}{\partial x_j}$, the notation $\ll\gg$ denotes the ensemble average associated with the dispersed phase, and $V_i\,(= \ll \hat{V}_i \gg)$ and v_i are the particle mean and fluctuating velocity, respectively. It is noted that, if U_i^* stands for the Eulerian mean fluid velocity at the particle position, $V_i = U_i^*$ is not a solution to Eq. (3.2). As a result, there always exists a relative mean velocity between the two phases which can result in large particle Reynolds numbers, especially far from the origin. In the next subsection, we consider particle Reynolds numbers small enough to set $f \equiv 1$. With this restriction, we show that an analytical expression can be found for the particle mean velocity gradient and that the dispersed phase is homogeneous. The more general case where $f = 1 + 0.15 Re_p^{0.687}$ will be considered in Section 3.2.

3.1. Homogeneous dispersed phase

For small particle Reynolds numbers, letting $f = 1$ in the averaged particle momentum Eq. (3.2) leads to:

$$\frac{D^V V_i}{Dt} = \frac{1}{\tau_p}\left(\ll \hat{U}_i^* \gg - V_i\right) - \ll v_j \frac{\partial v_i}{\partial x_j} \gg . \tag{3.3}$$

Provided that the initial particle velocity fluctuation is isotropic and the initial particle mean velocity is such that $V_\alpha(0) = \sigma_\alpha^0 x_\alpha(0)$ where σ_α^0 is a constant ($\alpha = 1, 2, 3$ with no summation on Greek indices), then we show that the following propositions are equivalent:

(i) The dispersed phase remains homogeneous.
(ii) The correlation $\ll v_j \frac{\partial v_i}{\partial x_j} \gg$ is identically zero.
(iii) $\exists \sigma_\alpha \forall t V_\alpha(x_j, t) = \sigma_\alpha(t) x_\alpha$.

Starting with the homogeneity (i) and isotropic initial condition assumptions, the directionality of the flow can only depend on the mean velocity gradient tensors $V_{i,j}$ and $U_{i,j}$. Hence, as $\ll v_j \frac{\partial v_i}{\partial x_j} \gg$ is a vector and represents a directional characteristic of the flow, it has to be zero (Blaisdell et al., 1991); see Appendix A for a proof.

Next, taking the correlation $\ll v_j \frac{\partial v_i}{\partial x_j} \gg$ to be zero and by substituting $\ll \hat{U}_i^* \gg$ by the Eulerian mean velocity for the surrounding fluid $U_i^* = U_{i,j} x_j$ (Barré, 1998 shows that the difference between $\ll \hat{U}_i^* \gg$ and U_i^* is small for cases considered in this study), from Eq. (3.3) we have

$$\frac{D^V x_i}{Dt} = V_i, \quad \frac{D^V V_i}{Dt} = \frac{1}{\tau_p}\left(U_{i,j} x_j - V_i\right). \tag{3.4}$$

These equations are combined to constitute second-order linear equations for x_i:

$$\frac{D^{V\,2}x_i}{Dt^2} + \frac{1}{\tau_p}\frac{D^V x_i}{Dt} - \frac{1}{\tau_p}U_{i,j}x_j = 0, \tag{3.5}$$

where $\frac{D^{V\,2}}{Dt^2} = \frac{D^V}{Dt}(\frac{D^V}{Dt})$. Eq. (3.5) are uncoupled and can be easily solved. The solution for $i = 1$ is

$$x_1 = c_1\exp(\xi_1 t) + c_2\exp(\eta_1 t), \tag{3.6}$$

where

$$\xi_1 = \frac{-1+\sqrt{1+4S\tau_p}}{2\tau_p}, \quad \eta_1 = \frac{-1-\sqrt{1+4S\tau_p}}{2\tau_p}. \tag{3.7}$$

For $i = 2$, the solution depends on a critical value for the particle time constant:

$$\tau_{p_{cr}} = \frac{1}{4S}. \tag{3.8}$$

For $\tau_p < \tau_{p_{cr}}$ the solution is

$$x_2 = c_3\exp(\xi_2 t) + c_4\exp(\eta_2 t), \tag{3.9}$$

where

$$\xi_2 = \frac{-1+\sqrt{1-4S\tau_p}}{2\tau_p}, \quad \eta_2 = \frac{-1-\sqrt{1-4S\tau_p}}{2\tau_p}. \tag{3.10}$$

For $\tau_p = \tau_{p_{cr}}$:

$$x_2 = (c_5 + c_6 t)\exp\left(\frac{-t}{2\tau_p}\right), \tag{3.11}$$

and for $\tau_p > \tau_{p_{cr}}$:

$$x_2 = \left[c_7\cos(\omega t) + c_8\sin(\omega t)\right]\exp\left(\frac{-t}{2\tau_p}\right), \tag{3.12}$$

where

$$\omega = \frac{\sqrt{\frac{\tau_p}{\tau_{p_{cr}}} - 1}}{2\tau_p}. \tag{3.13}$$

For $i = 3$, the solution of Eq. (3.5) leads to

$$x_3 = c_9\exp\left(\frac{-t}{\tau_p}\right) + c_{10}. \tag{3.14}$$

In Eqs. (3.6)–(3.14), c_i $(i = 1,\ldots,10)$ are integration constants. If $\tau_p < \tau_{p_{cr}}$, the solution in x_2-direction is similar to that in x_1-direction. For $\tau_p > \tau_{p_{cr}}$, an oscillatory solution with the

frequency ω is obtained in x_2-direction. In this case, the particles, due to their large inertia, are able to overcome the drag force and cross the x_1-axis. Once in the negative x_2 side of the (x_1, x_2)-plane, the particles are faced with an opposing flow. This results in a significant increase in the drag force and directs the particles back towards the x_1-axis. The mean velocity of the dispersed phase is determined from the solution for x_i, and is given in Appendix B for the initial condition $V_\alpha(0) = \sigma_\alpha^0 x_\alpha(0)$. It is observed, from Appendix B, that for any τ_p and for any direction there is a function $\sigma_\alpha(t)$ such that

$$V_\alpha(t) = \sigma_\alpha(t) x_\alpha(t), \tag{3.15}$$

where σ_α is a function of time only. This proves that (ii) results in (iii).

Finally, assuming (iii) the mean velocity gradient is defined by

$$V_{\alpha,\beta} = \sigma_\alpha(t)\delta_{\alpha\beta} \tag{3.16}$$

and the particle mean velocity is a solution for Eq. (3.4). Therefore, the equation for fluctuating velocity can be obtained by subtracting (3.4) from (3.1):

$$\frac{\mathrm{d}v_i}{\mathrm{d}t} = \frac{1}{\tau_p}\left(u_i^* - v_i\right) - V_{i,j} v_j. \tag{3.17}$$

The right-hand side of this Lagrangian equation depicts no explicit dependency on position, and is translationally invariant. Hence, and since the initial conditions consist of homogeneous turbulence, any statistical quantities formed from the fluctuating velocity will be invariant under such a transformation and the turbulence will remain homogeneous. This shows the constraint on the mean velocity gradient (iii) to be sufficient for the maintenance of homogeneity as stated in (i).

It has been shown that if the turbulence is homogeneous, the vector $\ll v_j \frac{\partial v_i}{\partial x_j} \gg$ is zero ((i) $\Rightarrow$ (ii)). Also, if this correlation vanishes, we have seen that the particle mean velocity satisfies $V_\alpha = \sigma_\alpha(t) x_\alpha$ for any t ((ii) $\Rightarrow$ (iii)). Finally, if the particle mean velocity gradient is a function of time only, then the turbulence remains homogeneous ((iii) $\Rightarrow$ (i)). Consequently the propositions (i), (ii), and (iii) are equivalent. From this we conclude that if the simulations are initialized in such a way that the particles fluctuating velocity field is isotropic and the particle mean velocity satisfies $V_\alpha = \sigma_\alpha^0 x_\alpha$ then the turbulence remains homogeneous and the mean velocity is $V_\alpha = \sigma_\alpha(t) x_\alpha$, for any t.

The solution for the mean velocity of the dispersed phase in three directions is summarized in Tables 1–3 for various cases. It is observed that for $\tau_p > \tau_{p_{cr}}$ the mean velocity gradient component in x_2-direction remains a periodic function of time, for any σ_2^0. For $\tau_p \le \tau_{p_{cr}}$, however, initially imposing $\sigma_1^0 = \xi_1$, $\sigma_2^0 = \xi_2$, and $\sigma_3^0 = 0$ results in

$$V_1 = \xi_1 x_1, \qquad V_2 = \xi_2 x_2, \qquad V_3 = 0, \quad \text{for any } t. \tag{3.18}$$

We also note that $\sigma_1 \to \xi_1$, $\sigma_2 \to \xi_2$, and $\sigma_3 \to 0$ for $t \to \infty$. Therefore, ξ_1, ξ_2 and 0 are the stable solutions for the particle mean velocity gradient components for $\tau_p \le \tau_{p_{cr}}$. Furthermore, notice that initializing the mean velocity field as $\sigma_1^0 = \eta_1$, $\sigma_2^0 = \eta_2$, and $\sigma_3^0 = -1/\tau_p$ also leads to a constant mean velocity gradient, $\sigma_\alpha(t) = \sigma_\alpha^0$. However, this corresponds to an unstable

Table 1
Particle mean velocity with isotropic initial conditions for fluctuations, in x_1-direction

$V_1(t) = \sigma_1(t)x_1, \sigma_1(0) = \sigma_1^0$		
Condition on τ_p	Initial condition	Solution for $V_{1,1}(t)$
any τ_p	$\sigma_1^0 \neq \xi_1$	$\sigma_1(t) = \frac{\eta_1 \exp(\eta_1 t) + \frac{\sigma_1^0 - \eta_1}{\xi_1 - \sigma_1^0}\xi_1 \exp(\xi_1 t)}{\exp(\eta_1 t) + \frac{\sigma_1^0 - \eta_1}{\xi_1 - \sigma_1^0}\exp(\xi_1 t)}$
		$\xi_1 = \frac{-1+\sqrt{1+4S\tau_p}}{2\tau_p}$
		$\eta_1 = \frac{-1-\sqrt{1+4S\tau_p}}{2\tau_p}$
	$\sigma_1^0 = \xi_1$	$\sigma_1(t) = \xi_1 = \text{constant}$

Table 2
Particle mean velocity with isotropic initial conditions for fluctuations, in x_2-direction

$V_2(t) = \sigma_2(t)x_2, \sigma_2(0) = \sigma_2^0$		
Condition on τ_p	Initial condition	Solution for $V_{2,2}(t)$
$\tau_p < \tau_{p_{cr}}$	$\sigma_2^0 \neq \xi_2$	$\sigma_2(t) = \frac{\eta_2 \exp(\eta_2 t) + \frac{\sigma_2^0 - \eta_2}{\xi_2 - \sigma_2^0}\xi_2 \exp(\xi_2 t)}{\exp(\eta_2 t) + \frac{\sigma_2^0 - \eta_2}{\xi_2 - \sigma_2^0}\exp(\xi_2 t)}$
$(\tau_{p_{cr}} = \frac{1}{4S})$		$\xi_2 = \frac{-1+\sqrt{1-4S\tau_p}}{2\tau_p}$
		$\eta_2 = \frac{-1-\sqrt{1-4S\tau_p}}{2\tau_p}$
	$\sigma_2^0 = \xi_2$	$\sigma_2(t) = \xi_2 = \text{constant}$
$\tau_p = \tau_{p_{cr}}$	$\sigma_2^0 \neq -\frac{1}{2\tau_p}$	$\sigma_2(t) = \frac{\sigma_2^0 - \left(\sigma_2^0 + \frac{1}{2\tau_p}\right)\frac{t}{2\tau_p}}{1 + \left(\sigma_2^0 + \frac{1}{2\tau_p}\right)t}$
	$\sigma_2^0 = -\frac{1}{2\tau_p}$	$\sigma_2(t) = -\frac{1}{2\tau_p} = \text{constant}$
$\tau_p > \tau_{p_{cr}}$	any σ_2^0	$\sigma_2(t) = \frac{\sigma_2^0 + \frac{-1}{2\tau_p\omega}(\sigma_2^0 + 2S)\tan(\omega t)}{1 + \frac{\sigma_2^0 + \frac{1}{2\tau_p}}{\omega}\tan(\omega t)}$
		$\omega = \frac{\sqrt{4S\tau_p - 1}}{2\tau_p}$

Table 3
Particle mean velocity with isotropic initial conditions for fluctuations, in x_3-direction

$V_3(t) = \sigma_3(t)x_3$, $\sigma_3(0) = \sigma_3^0$		
Condition on τ_p	Initial condition	Solution for $V_{3,3}(t)$
any τ_p	$\sigma_3^0 \neq 0$	$\sigma_3(t) = \frac{\exp\left(\frac{-t}{\tau_p}\right)}{\frac{1+\tau_p\sigma_3^0}{\sigma_3^0} - \tau_p\exp\left(\frac{-t}{\tau_p}\right)}$
	$\sigma_3^0 = 0$	$\sigma_3(t) = 0$

equilibrium solution for $V_{i,j}$, and any small perturbation would make the mean velocity of the dispersed phase to diverge from this solution.

The above discussion indicates that for small Re_p the particle mean velocity is known. Therefore, to calculate the statistics of the dispersed phase in this case, we only need to solve the fluctuating velocity equation in the fixed coordinates:

$$\frac{dv_i}{dt} = \frac{1}{\tau_p}\left(u_i^* - v_i\right) - V_{i,j}v_j, \tag{3.19}$$

with

$$\frac{d\hat{X}_i}{dt} = v_i + \sigma_j(t)\hat{X}_j\delta_{ij}. \tag{3.20}$$

It must be noted that the relative mean velocity, and therefore Re_p, increases with the distance from the origin. Thus, the study of the homogeneous dispersed phase is restricted to a final physical domain surrounding the origin. However, this domain has to be large enough to encompass the large scales of turbulence. During the present simulations, this requirement is satisfied in all three directions and for all the particle time constants considered as the domain size remains greater than three times the flow integral length scale ($l = \frac{\pi}{2u'^2}\int_0^\infty \frac{E(\kappa)}{\kappa}d\kappa$ with κ and $E(\kappa)$ denoting the wavenumber and the energy spectrum of the carrier phase, respectively) at any time (see Table 4).

Table 4
Variation of the ratio of the carrier phase integral length scale to the dispersed phase computational box size (L_i denotes the box size in the x_i-direction) for different particle time constants during the plane strain simulations

τ_p	0.112	0.225	0.372	0.434
l/L_1	0.047→ 0.085	0.050→ 0.085	0.052→ 0.085	0.057→ 0.085
l/L_2	0.021→ 0.183	0.021→ 0.229	0.021→ 0.275	0.021→ 0.366
l/L_3	0.042→ 0.088	0.042→ 0.088	0.042→ 0.088	0.042→ 0.088

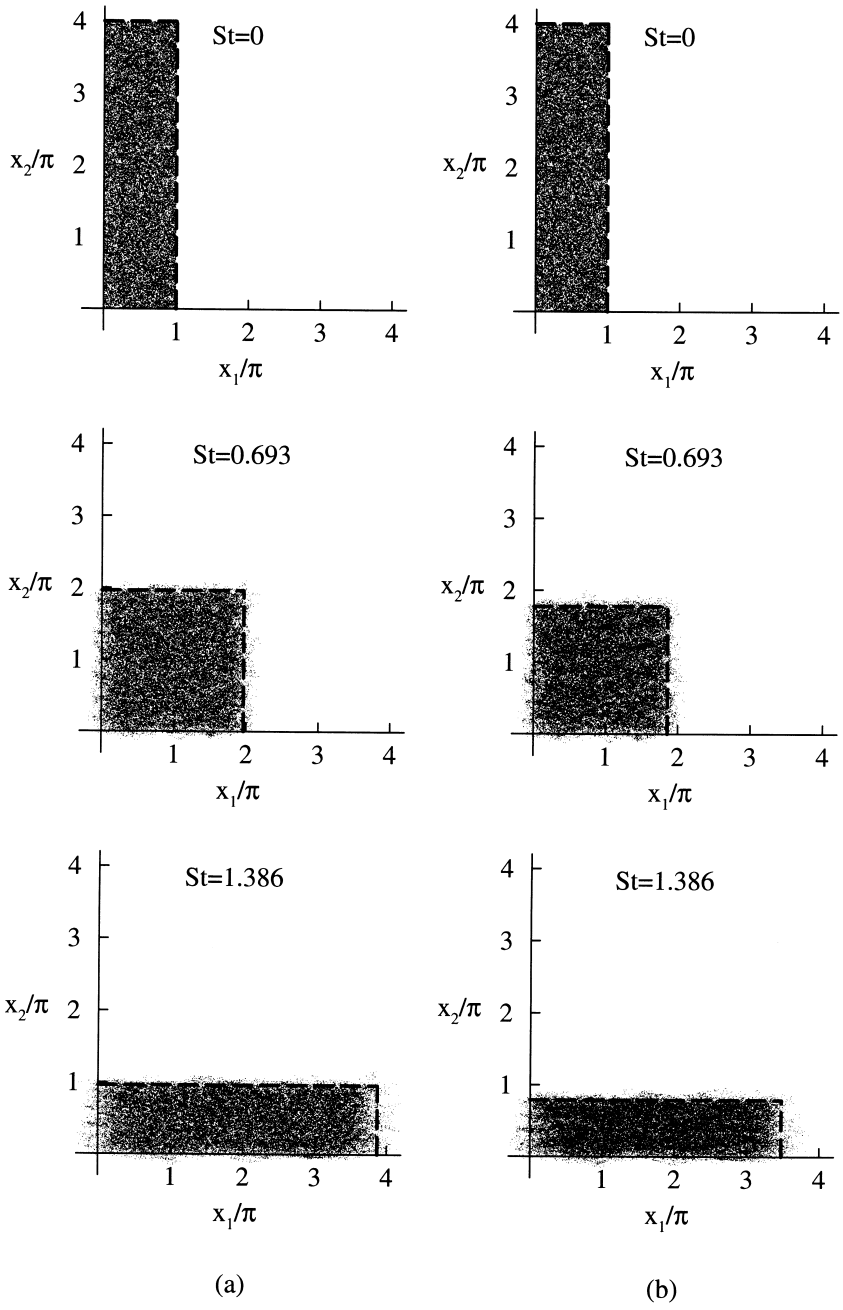

Fig. 2. Instantaneous particle distribution at various times for (a) $\tau_p = 0.1\tau_{p_{cr}}$ and (b) $\tau_p = 0.5\tau_{p_{cr}}$. The prediction of the theory for the particle-containing box is also shown with dashed lines.

The validity of the analysis presented in this section for the mean velocity of the dispersed phase is tested in our numerical simulations by plotting the instantaneous locations of all the particles at various times. For this purpose, using the fluid velocity calculated by DNS (see Section 4), we integrate the instantaneous (total) particle velocity equation (see Eq. (3.21) below). The particle distribution obtained in this manner is independent of the above analysis and is shown in Fig. 2 for two different particle sizes (note that in the figure the inverse of the mean velocity gradient, S, has been used to normalize the time). At the same time, starting from a mean particle velocity (and its corresponding initial conditions) given by Eq. (3.18), the temporal evolution of the 'particle-containing' box can be predicted analytically. This prediction is also shown in Fig. 2 and is compared to the particle domain formed by solving the equation for the instantaneous velocity in the numerical simulation. A close agreement is observed and only a small portion of particles are dispersed (by turbulence fluctuations) outside the predicted box at the final simulation time. Fig. 2 also shows that the size of the particle-containing box decreases in time, a phenomenon more visible for larger particles. This demonstrates the 'compressibility' of the dispersed phase which has been captured here by the plane strain flow.

3.2. Inhomogeneous dispersed phase

When the particle Reynolds number is large, the preceding formulation is not justified. The correction to drag, $f = 1 + 0.15Re_p^{0.687}$, introduces a nonlinear and explicit dependency on

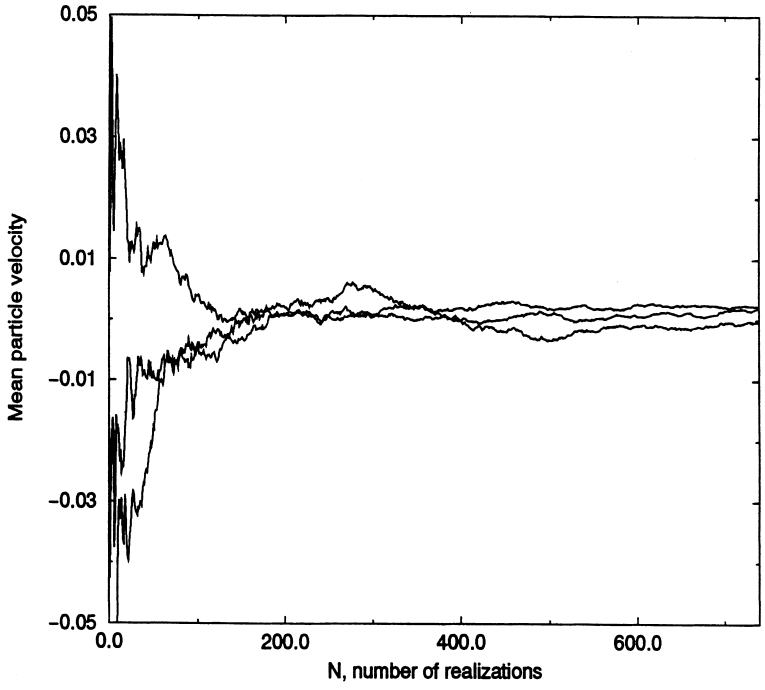

Fig. 3. 'Double-averaged' particle mean velocity at three particle locations ($t = 0$).

position in the particles equations of motion. Hence the dispersed phase cannot be considered homogeneous, except in x_3-direction. Because of the relatively short length of the domain along this axis, averaging in x_3-direction only is not sufficient to obtain accurate statistics. It is still possible to increase the number of realizations by repeating the simulation, starting with different initial conditions. But the number of simulations required to achieve a good accuracy may be large.

To estimate the number of repetitions of the simulation necessary to compute statistics, 1000 initial turbulent flow fields are generated and particle velocities at $t = 0$ are averaged over cells in x_3-direction. Then the averaging over the number of simulations is performed. For this estimation, the particle distribution is kept the same for all the repetitions and no particle mean velocity is imposed, thus the averaged particle velocity should converge to zero. We also emphasize that the simulations are stopped after the first time step. Consequently, only statistical errors are estimated, without physical consideration. Fig. 3 shows the 'double-averaged' mean particle velocity as a function of the number of simulations used for averaging, for three typical particle locations. It is observed that over 100 repetitions of the same simulation are required in order to achieve a reasonable accuracy in the calculation of the mean particle velocity. This is not affordable with the current computer resources available (although we expect that statistics evaluated at longer times would provide a faster convergence due to the dynamics of the turbulence and the velocity correlations). Therefore, the results of our simulations for large Re_p are only used to investigate the dispersion characteristics of the particles. For inhomogeneous dispersed phase, the particle mean velocity is not known and we solve the instantaneous particle equations:

$$\frac{d\hat{X}_i}{dt} = \hat{V}_i, \quad \frac{d\hat{V}_i}{dt} = \frac{f}{\tau_p}\left(\hat{U}_i^* - \hat{V}_i\right), \tag{3.21}$$

in the fixed coordinates.

4. Overview of simulations

A Fourier pseudospectral method with triply periodic boundary conditions is employed for the spatial representation of the fluid velocity and pressure. All calculations for the carrier phase are performed in the Fourier space with the exception of the non-linear terms. Aliasing errors are treated by truncating energies outside of a spherical wavenumber shell having radius $\sqrt{2}N/3$, (where N is the number of grid points in any direction) and time advancement is performed using an explicit second order accurate Adams–Bashford method. Temporal advancement of the Lagrangian particle equations is also done by the Adams–Bashford method. In order to evaluate fluid variables at the particle locations a fourth-order accurate Lagrange polynomial interpolation scheme is employed.

The initial conditions for the plane strain runs are obtained by preliminary simulations of homogeneous decaying turbulence. The initial (random) velocity field for the carrier phase, in decaying simulations, is generated in the Fourier space. The method of initialization is the same as that used by Rogallo and Moin (1984) and Lee and Reynolds (1985). In this method,

one supplies the resolution of the energy-containing eddies ($\mathcal{N}_\Lambda$) and the smallest eddies ($\mathcal{N}_\eta$) in a given computational domain. Then the energy spectrum function and the box Reynolds number, Re_0, are determined. The energy spectrum is constructed as:

$$E(\kappa) = \begin{cases} \gamma\kappa^2 & \text{if } \kappa_0 \le \kappa \le \kappa_p \\ \gamma\kappa_p^{\frac{11}{3}}\kappa^{\frac{-5}{3}} & \text{if } \kappa_p \le \kappa \le \kappa_c \\ 0 & \text{otherwise} \end{cases} \tag{4.1}$$

where γ and κ_p are determined from the values of $\mathcal{N}_\Lambda$, $\mathcal{N}_\eta$ and N (Lee and Reynolds, 1985). Here, we choose $\mathcal{N}_\Lambda = 5.7$, $\mathcal{N}_\eta = 0.35$ and $N = 96$, leading to $\gamma = 2.655 \times 10^{-4}$, $\kappa_p = 11$ and $Re_0 = 232$.

The computational domain is elongated (shortened) in the direction of positive (negative) mean strain rates during plane strain runs (Fig. 1). Therefore, if we begin with isotropic mesh configuration with three identical sides, the mesh aspect ratio, defined as the ratio of the longest side of the mesh to the shortest, increases in time. As the mesh aspect ratio increases, it becomes difficult to resolve turbulence equally in every direction. Hence, computation must be stopped at relatively short times. To allow the simulations continue for a longer time, we implement a predistorted initial mesh with short side in the direction to be elongated by positive mean strain rate and vice versa. Therefore, the mesh aspect ratio for the decay of isotropic turbulence is 1/2:2:1, and the simulations are conducted within the domain $0 \le x_1 \le \pi$, $0 \le x_2 \le 4\pi$, $0 \le x_3 \le 2\pi$. The particles are initially distributed randomly throughout this domain, and are specified to have zero velocity difference with the local fluid ($v_i\ (t=0) = u_i^*\ (t=0)$). The decaying simulations are stopped when the higher-order statistics approximately reach their asymptotic values. Then the plane strain simulations are started, with the turbulent velocity fields and the particle distributions taken from the decaying

Table 5
Parameters and initial conditions used in the plane strain simulations

Carrier phase									
$\eta_k\kappa_{max}$	τ_k	v_k	u'	l	q^2	ϵ	Re_T	S	$\tilde{S}$
1.40	0.225	0.138	0.198	0.268	0.118	0.084	39	0.739	1.0
Dispersed phase									
τ_p	τ_p/τ_k	$\tau_p/\tau_{p_{cr}}$	v'	q_p^2	$\ll Re_p \gg$	$V_{1,1}$	$V_{2,2}$	$V_{3,3}$	statistics
0.112	0.5	0.33	0.199	0.119	0.05	0.686	-0.739	0	yes
0.225	1	0.66	0.199	0.119	0.12	0.645	-0.739	0	yes
0.372	1.65	1.09	0.197	0.117	0.24	0.603	-0.739	0	yes
0.434	1.9	1.28	0.198	0.116	0.29	0.588	-0.739	0	yes
0.507	2.2	1.5	-	-	0.36	0.572	-0.739	0	no
0.675	3	2	-	-	0.53	0.541	-0.739	0	no
1.126	5	3.3	-	-	1.00	0.479	-0.739	0	no
1.691	7.5	5	-	-	1.58	0.428	-0.739	0	no

turbulence runs. For the carrier phase, the initial aspect ratio for the computational domain is 1/2:2:1 ($B_{11}^0=2$, $B_{22}^0=1/2$, $B_{33}^0=1$), and at the final simulation time this becomes 2:1/2:1 ($B_{11}=1/2$, $B_{22}=2$, $B_{33}=1$). That is, if we define the reference total strain as $c=\exp(St)$, each strain run is performed until the reference total strain reaches approximately 4.

For a given mean strain rate ($S = 0.739$), we have considered eight cases to investigate the effects of the particle time constant, using 1.2×10^5 particles on 96^3 grid points. For all the simulations $\rho_p = 721.8$ is used. Primarily, we performed several simulations of the decaying isotropic turbulence, in order to establish initial conditions for the plane strain runs. The flow parameters considered in the plane strain simulations are given in Table 5, along with additional information pertaining to initial conditions. In this table, κ_{max} denotes the highest wavenumber resolved after dealiasing, η_k, τ_k and v_k represent the Kolmogorov length, time and velocity scales, respectively, and u' is the rms of the fluctuating velocity. Also, $q^2=2k=\langle u_iu_i\rangle$ is twice of the fluid turbulence kinetic energy, $\epsilon=2\nu\langle s_{ij}s_{ij}\rangle$ is the mean dissipation, where the symmetric rate of strain tensor is $s_{ij}=(\partial u_i/\partial x_j+\partial u_j/\partial x_i)/2$, $Re_T=q^4/\epsilon\nu$ denotes the turbulence Reynolds number, and $\tilde{S}=Sq^2/\epsilon$ is the mean strain rate parameter ($\tilde{S}$ is the ratio of the time scale of distortion of turbulence to that of the mean flow). To demonstrate the accuracy of the single phase flow simulation, a comparison is provided in Table 6 between some of the present DNS results with those from the DNS of Rogallo and Moin (1984) and Lee and Reynolds (1985) and the experiment of Tucker and Reynolds (1968). In Table 6, $a_{ij}^f=\langle u_iu_j\rangle/k-2/3\ \delta_{ij}$ is the fluid anisotropy tensor.

Table 5 also provides a listing of the cases considered to study the effects of the particle time constant. For each case, it is indicated whether or not statistics of particle fluctuating velocity are calculated, that is whether the particle Reynolds numbers remain small enough during the simulation to consider the dispersed phase to be homogeneous. The corresponding initial values of the r.m.s. of the dispersed phase fluctuating velocity, v', and twice of the turbulence kinetic energy, $q_p^2=2k_p=\ll v_iv_i\gg$ (for the homogeneous dispersed phase cases), and the averaged particle Reynolds number $\ll Re_p\gg$ are given. The mean velocity gradient of the dispersed phase is initially imposed as:

Table 6
Comparison of the present single phase flow results with previous simulations of Lee and Reynolds (1985) (LR) and Rogallo and Moin (1984) (RM) and the experiments of Tucker and Reynolds (1968) (TR)

	Present results	LR	RM	TR
c	4.0	4.0	4.0	4.0
Re_T	61	69	241	1000
$\tilde{S}$	1.0	1.0	1.0	0.9
a_{11}^f	-0.507	-0.516	-0.433	-0.391
a_{22}^f	0.496	0.538	0.508	0.316
a_{33}^f	0.015	-0.003	-0.036	0.083

$$V_{i,j}(0) = \begin{pmatrix} \xi_1 & 0 & 0 \\ 0 & -S & 0 \\ 0 & 0 & 0 \end{pmatrix}.$$

In this manner, for homogeneous dispersed phase $V_{i,j}(t) = V_{i,j}(0) = \text{constant}$ for any t, if $i \neq 2$ and $j \neq 2$. Also, $V_{2,2}(t, \tau_{p_1}) \leq V_{2,2}(t, \tau_{p_2})$ if $\tau_{p1} < \tau_{p2}$ for the range of time considered in the present simulations. Notice that, to keep the particle Reynolds number small, in both homogeneous and inhomogeneous dispersed phase cases, the mean velocity difference in x_2-direction is zero when the plane strain runs start.

5. Results

In this section, we present the results of the simulations for both homogeneous and inhomogeneous dispersed phase. As mentioned earlier, only for homogeneous dispersed phase we are able to calculate the statistics that require the knowledge of the mean velocity of the dispersed phase. These include the velocity autocorrelation coefficient, the Reynolds stress, the turbulence kinetic energy, the anisotropy tensor, and the mean relative fluctuating velocity.

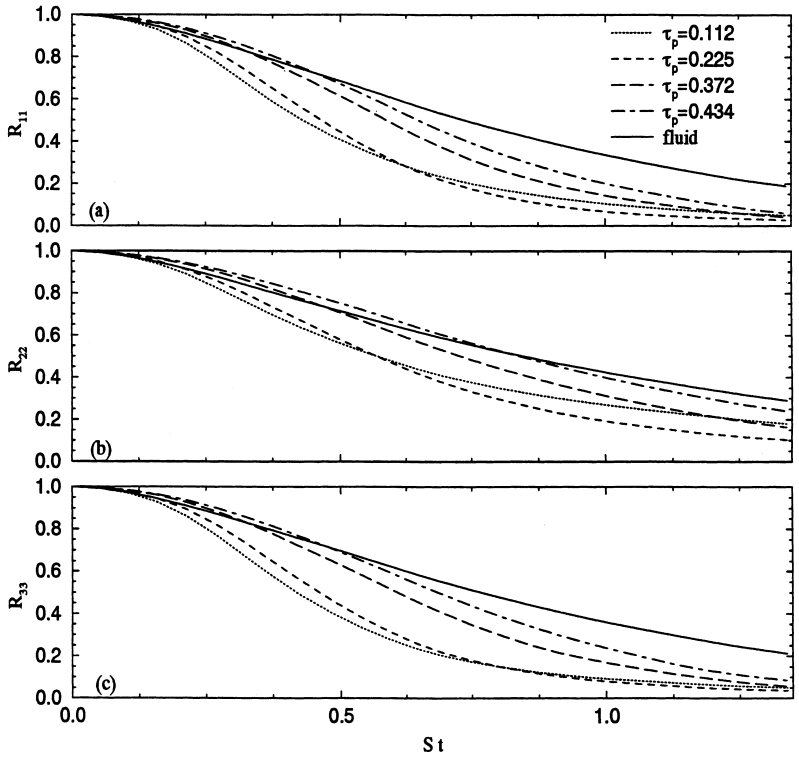

Fig. 4. Effect of τ_p on the particle velocity autocorrelation and comparison with the fluid velocity autocorrelation; (a) in the elongated direction x_1, (b) in the shortened direction x_2, (c) in the spanwise direction x_3.

First, we discuss the results for cases in which the dispersed phase can be considered homogeneous. For these cases, the Lagrangian autocorrelation coefficient of the particle velocity is defined as:

$$R_{\alpha\alpha}(t) = \frac{\ll v_\alpha(t_0)v_\alpha(t_0+t) \gg}{\ll v_\alpha^2(t_0) \gg^{\frac{1}{2}} \ll v_\alpha^2(t_0+t) \gg^{\frac{1}{2}}}, \quad \alpha = 1, 2, 3 \tag{5.1}$$

where t_0 is the time at which we start computing the Lagrangian statistics. Since the turbulence is non-stationary, the value of $R_{\alpha\alpha}$ depends on the choice of t_0. The total time in our plane strain simulations is somewhat short, therefore, we choose to take $t_0 = 0$ which is the starting time for plain strain simulations. The autocorrelation coefficient for various τ_p values are shown in Fig. 4 along with that of the massless fluid particle. It is observed that, for short dispersion times, the 'memory' of the particle to its previous velocity is increased as the particle inertia increases, thus increasing the autocorrelation coefficient. For $\tau_p > \tau_{p_{cr}} (= 0.338)$ the magnitude of the particle autocorrelation exceeds that of the fluid particle. At later times, the autocorrelation of these heavier particles cross over that of the fluid such that at long times the particle velocities are less correlated than the fluid velocities. This is again due to the particle inertia. At long times, the solid particle continues to interact with new fluid elements and thus $R_{\alpha\alpha}$ decays at a faster rate than that of the fluid. In all three directions, a crossing is observed for the autocorrelation curves of various τ_p. The crossing occurs sooner in the x_2-direction and for the autocorrelation curves of $\tau_p = 0.112$ and $\tau_p = 0.225$. This suggests that particles with high inertia change their surrounding fluid more rapidly and tend to lose correlation with their previous velocity faster than lighter particles. In plane strain flows, the particle mean velocity depends on the particle time constant and in our simulations the relative mean velocity between the particle and its surrounding fluid increases with the increase of τ_p. Thus particles with higher inertia are more subjected to 'crossing-trajectories' effects than lighter ones, and the decay rate of $R_{\alpha\alpha}$ increases with τ_p at long times causing the autocorrelation to become smaller for larger particle time constant. Fig. 4 also shows that the autocorrelation of the particle velocity in the shortened direction (x_2) is larger than that in both elongated (x_1) and spanwise (x_3) directions.

Another interesting phenomenon observed in Fig. 4 is that the variation of the autocorrelation with the particle time constant is not monotonic. For example, the long time value of R_{11}, in Fig. 4a, decreases with the decrease of τ_p to 0.225 and then increases with further decrease of τ_p. This could be due to the crossing-trajectories effects and the preferential distribution of the particles in high-strain-rate regions of the flow. A similar phenomenon is observed by Wang and Maxey (1993) for the settling velocity of particles in the presence of gravity in isotropic turbulence. They observe a peak value in the variation of the 'increase in the particle mean settling velocity' when the particle time constant is close to the Kolmogorov time scale of the turbulence. It should also be noted that the flow considered here is non-stationary and the dispersed phase exhibits compressibility effects and there is a significant variation in the mean concentration in time. These could also contribute to the non-monotonic behavior observed in the figure and demand more future exploration.

The temporal variation of the normal Reynolds stresses of the fluid ($\langle u_\alpha^2 \rangle$) and particles ($\ll v_\alpha^2 \gg$), and the fluid–particle velocity covariance ($\ll u_\alpha^* v_\alpha \gg$) are shown in Fig. 5. The

particle Reynolds stress in x_2-direction ($\ll v_2^2 \gg$) is strongly affected by the mean velocity gradient. It is considerably larger than the corresponding fluid-particle velocity covariance ($\ll u_2^* v_2 \gg$), and exceeds the fluid Reynolds stress ($\langle u_2^2 \rangle$). These features are even more pronounced when the particle time constant increases. It is also observed that an increase of particle inertia decreases the fluid–particle velocity covariance, below the value of $\langle u_2^2 \rangle$, due mainly to strong decorrelation of the fluid and particle velocities at larger τ_p. These results are in general agreement with theoretical results of Reeks (1993) and Liljegren (1993) and numerical results of Mashayek (1998) regarding the effect of a mean fluid velocity gradient on the streamwise particle velocity variance in shear flows. However, the non-zero mean fluid velocity gradient component in the stretched direction ($U_{1,1} = S$) does not affect $\ll v_1^2 \gg$ similarly to that in the squeezed (x_2) direction. In the analysis of Liljegren (1993) the term

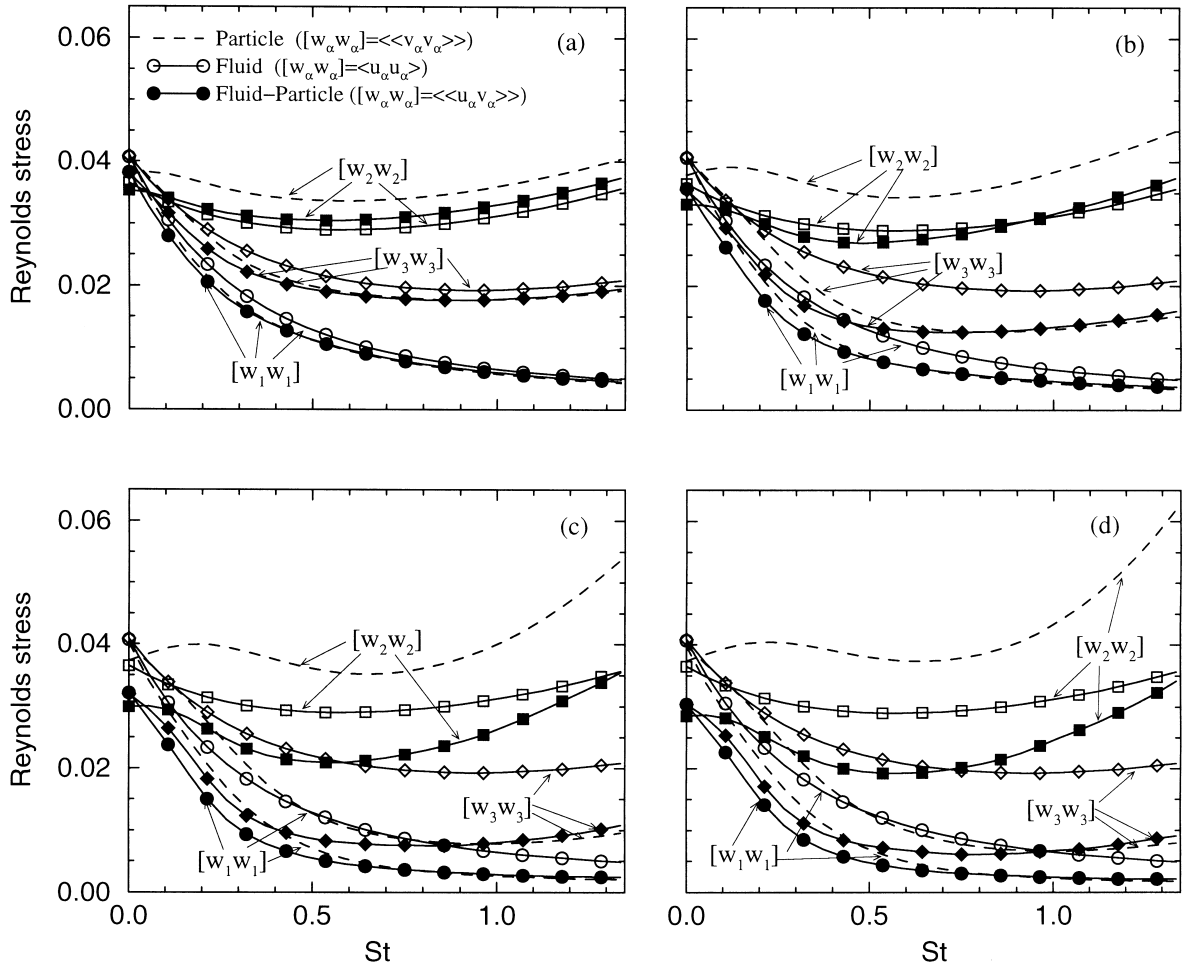

Fig. 5. Temporal evolution of the Reynolds stress components of the fluid and the particles and the fluid-particle covariance. Hollow and filled symbols refer to the fluid and the fluid-particle, respectively. (a) $\tau_p = 0.112$, (b) $\tau_p = 0.225$, (c) $\tau_p = 0.372$, and (d) $\tau_p = 0.434$.

responsible for the increase of the streamwise particle velocity variance above the fluid one is proportional to $-V_{1,2} \ll v_1 v_2 \gg$ which is positive in the case of shear flow. Here, the fluid mean velocity gradient results in a positive particle mean velocity gradient component $V_{1,1}$. Thus, the term $-V_{1,1} \ll v_1^2 \gg$ in the transport equation of $\ll v_1^2 \gg$ behaves like a dissipation and decreases the particle Reynolds stress in x_1-direction below that in x_3-direction. Moreover, $V_{1,1}$ is larger than $U_{1,1}$ and increases with particle inertia. This could explain that the particle velocity variance in the elongated direction is smaller than the fluid one and decreases with increasing τ_p (although a direct analogy with Liljegren (1993) theory is not attempted here). In the spanwise direction, the particle velocity variance is not directly affected by the mean velocity gradients and consistent with the results for shear flow in the normal or spanwise

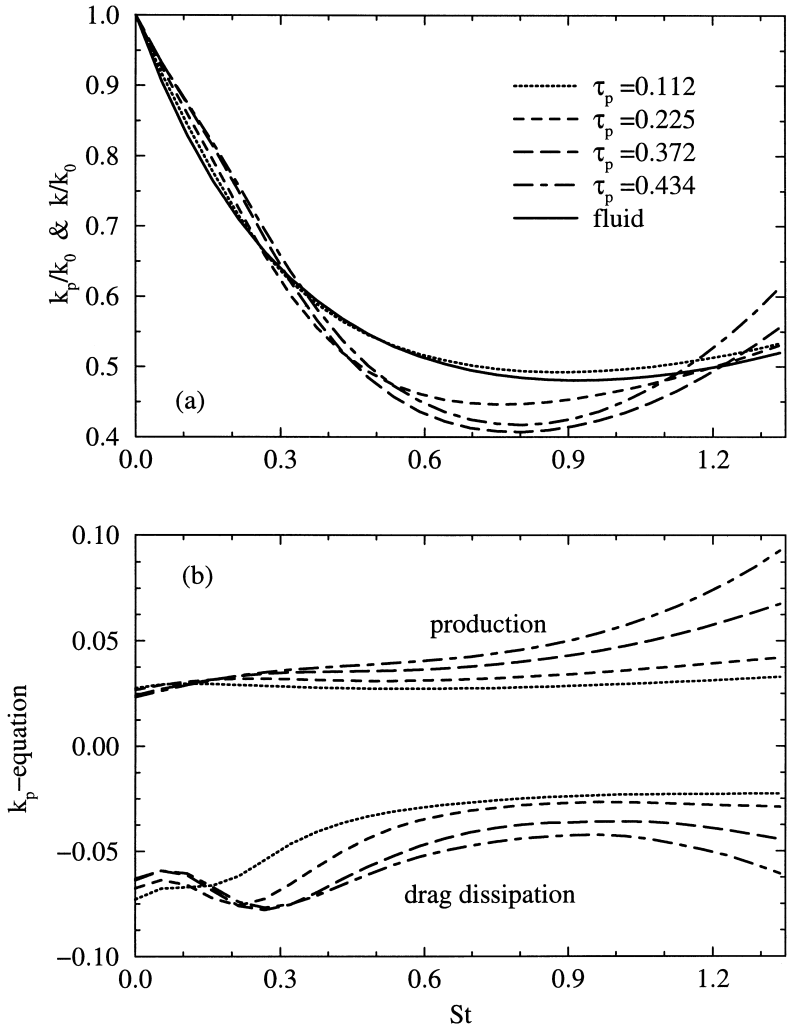

Fig. 6. Temporal variations of (a) the normalized turbulence kinetic energy for the fluid and the particles, and (b) the production and drag dissipation terms appearing in the particle turbulence kinetic energy Eq. (5.2).

directions, it remains below the corresponding fluid turbulent stresses and, given sufficient development time, becomes nearly equal to the fluid–particle velocity covariance. An inspection of Fig. 5 shows that the particle velocity variance in the spanwise direction decreases when the particle time constant increases.

The effects of the particle inertia on the evolution of the particle turbulence kinetic energy appear in Fig. 6a. All the kinetic energies shown in this figure are normalized by k_0, the turbulence kinetic energy of the fluid at the initial time. It is observed that during the early dispersion times, the normalized particle turbulence kinetic energy is larger than the fluid one, and increases with the increase of particle inertia. Later, the fluid turbulence kinetic energy starts to level off and k_p continues to decay at a faster rate than k. Because the decay rate of k_p is larger for smaller inertia particles, the time at which the particle turbulence kinetic energy decreases below that of the fluid is shorter for smaller particles. At long dispersion times, the particle turbulence kinetic energy increases over that of the fluid for all cases. Increasing the particle time constant results in a larger growth rate for the particle turbulence kinetic energy for long times.

To explain the trends observed in Fig. 6a, we consider the transport equation for the particle turbulence kinetic energy:

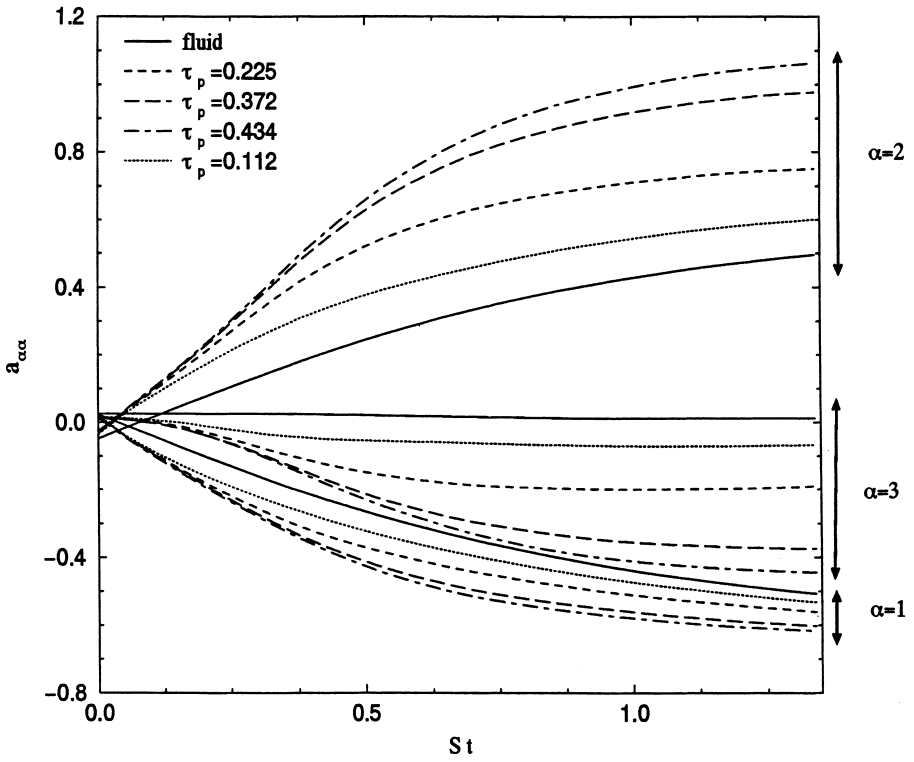

Fig. 7. Temporal variations of the anisotropy tensor components of the fluid and the particles.

$$\frac{D^V k_p}{Dt} = -\left(V_{1,1} \ll v_1^2 \gg + V_{2,2} \ll v_2^2 \gg\right) + \frac{1}{\tau_p}\left(\ll u_i^* v_i \gg -2k_p\right). \tag{5.2}$$

The expression $-(V_{1,1} \ll v_1^2 \gg + V_{2,2} \ll v_2^2 \gg)$ on the right-hand side of Eq. (5.2) represents a production by the mean velocity gradient, whereas the last two terms indicate the drag contribution. The temporal evolution of these terms in Fig. 6b indicates that for all the cases the term due to drag always acts like a dissipation and tends to counterbalance the production. During the initial times, the dissipation overcomes the production and the particle turbulence kinetic energy experiences a rapid decay, similar to that of the fluid, as shown in Fig. 6a. At longer times, the dominance of the drag dissipation over the production is overturned. The time of overturning becomes slightly longer as the particle time constant increases. Fig. 6b also shows that, at long times, the increase of τ_p results in the increase of both the production and the dissipation. However, the increase of the production with the particle time constant occurs with a faster rate than that of the dissipation. As a result, the growth rate of the particle turbulence kinetic energy is increased with the increase of the particle time constant, in contrast to initial times that the decay rate of k_p decreases with the increase of τ_p.

Fig. 7 illustrates the temporal variations of the diagonal (normal) components of the anisotropy tensor for both the carrier and the dispersed phases. Here, the anisotropy tensor for the dispersed phase, $a_{ij}^p = \ll v_i v_j \gg / k_p - 2/3\delta_{ij}$, is defined similarly to that of the carrier phase. All of the off-diagonal (shear) components are zero in plane strain flow. Due to initial (nearly) isotropic conditions, all the components are approximately equal to zero at $t = 0$ (although we note a slight anisotropy generated during the decaying turbulence runs). In time, the action of the mean velocity gradient increases the energy component in the shortened direction (x_2, with a negative mean velocity gradient), and decreases the energy in the elongated direction (x_1, with a positive mean velocity gradient). In the absence of a production mechanism, the component in x_3-direction tends to decay. However, the fluid pressure redistributes the energy among the components, and after some initial time equilibrium values are approached. A similar behavior is also observed for the dispersed phase. It is clearly observed that the anisotropy of the dispersed phase is substantially larger than that of the fluid. This is due mainly to the lack of a mechanism similar to pressure in the fluid phase by which energy may be exchanged among various components in the dispersed phase. The extent of the anisotropy of the carrier phase is, however, bounded at long times by the action of the drag force. The

Table 7
Number of time constants required by the particles to reach the peak in $\ll (u_i^* - v_i)^2 \gg / \ll (u_i^*)^2 \gg$

τ_p	t_{peak}/τ_p		
	$i = 1$	$i = 2$	$i = 3$
0.112	3.38	3.01	3.38
0.225	2.09	2.16	2.09
0.372	1.29	1.53	1.29
0.434	1.15	1.49	1.15

variation of the anisotropy tensor components with the increase of the particle inertia is in agreement with previous results for homogeneous turbulent shear flows — the anisotropy in the particle phase increases with the increase of the particle time constant (Taulbee et al., 1999; Mashayek, 1998).

The mean-square relative fluctuating velocity, $\ll (u_i^* - v_i)^2 \gg$, is a measure of the deviation of the particle velocity fluctuation from that of the surrounding fluid. The temporal variation of the mean-square relative velocity is also used to determine the time at which the particles become independent of their initial conditions — Riley and Patterson (1974) chose the time of occurrence of the peak of $\ll (u_i^* - v_i)^2 \gg$ as the time at which the particles have adjusted to decaying turbulence. Fig. 8 shows the variations of this quantity normalized by the surrounding fluid mean-square velocity $\ll (u_i^*)^2 \gg$ for various τ_p. The evolution of $\ll (u_i^* - v_i)^2 \gg / \ll (u_i^*)^2 \gg$ is similar in the three directions and the peak time, t_{peak}, is approximately the same for $i = 1$, 2, and 3. As expected from the results for Lagrangian autocorrelations, for increasing τ_p the influence of the initial condition of the particle velocity is more significant and

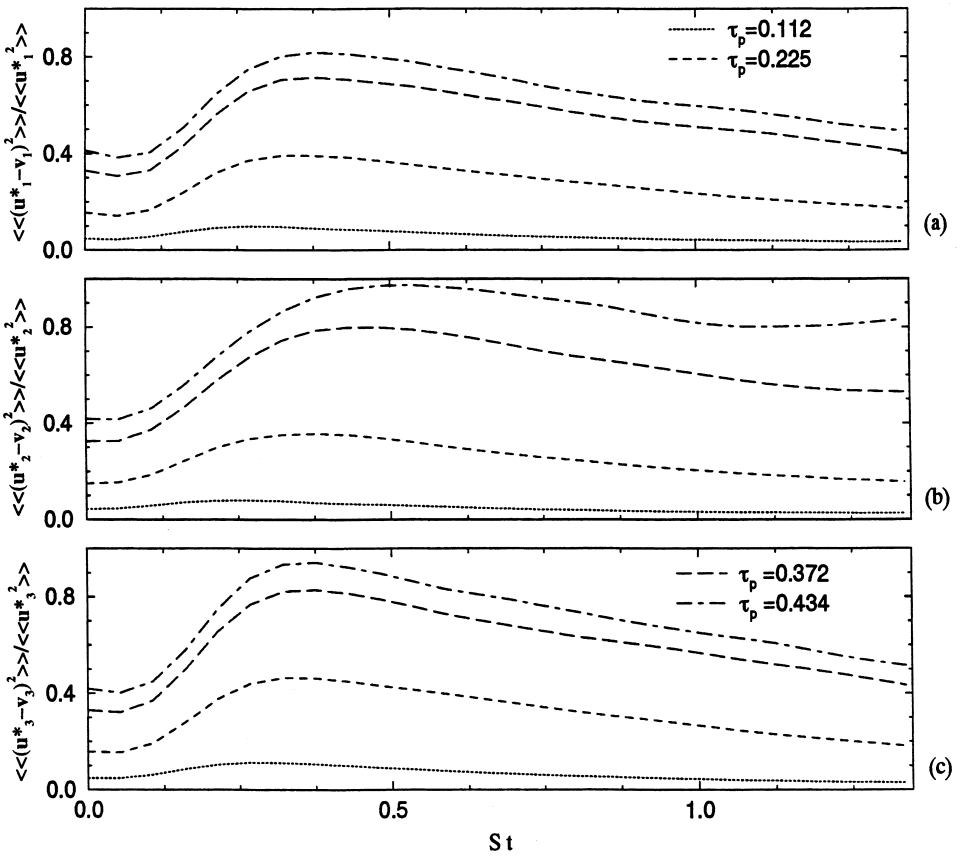

Fig. 8. Temporal evolution of the mean-square relative fluctuating velocity; (a) in the elongated direction x_1, (b) in the shortened direction x_2, (c) in the spanwise direction x_3.

t_{peak} is larger. However, if t_{peak} is normalized by τ_p, we observe that the lighter the particle, the larger t_{peak}/τ_p. The number of time constants required for each particle to reach the peak in various directions is shown in Table 7. In general, the magnitude of $\ll (u_i^* - v_i)^2 \gg / \ll (u_i^*)^2 \gg$ increases with the increase of τ_p due to the larger slip velocity experienced by the heavier particles. It is interesting to note that for long dispersion times and for all the cases considered, we have:

$$\frac{\ll (u_1^* - v_1)^2 \gg}{\ll (u_1^*)^2 \gg} \leq \frac{\ll (u_3^* - v_3)^2 \gg}{\ll (u_3^*)^2 \gg}, \tag{5.3}$$

whereas

$$\frac{\ll (u_2^* - v_2)^2 \gg}{\ll (u_2^*)^2 \gg} \leq \frac{\ll (u_3^* - v_3)^2 \gg}{\ll (u_3^*)^2 \gg}, \tag{5.4}$$

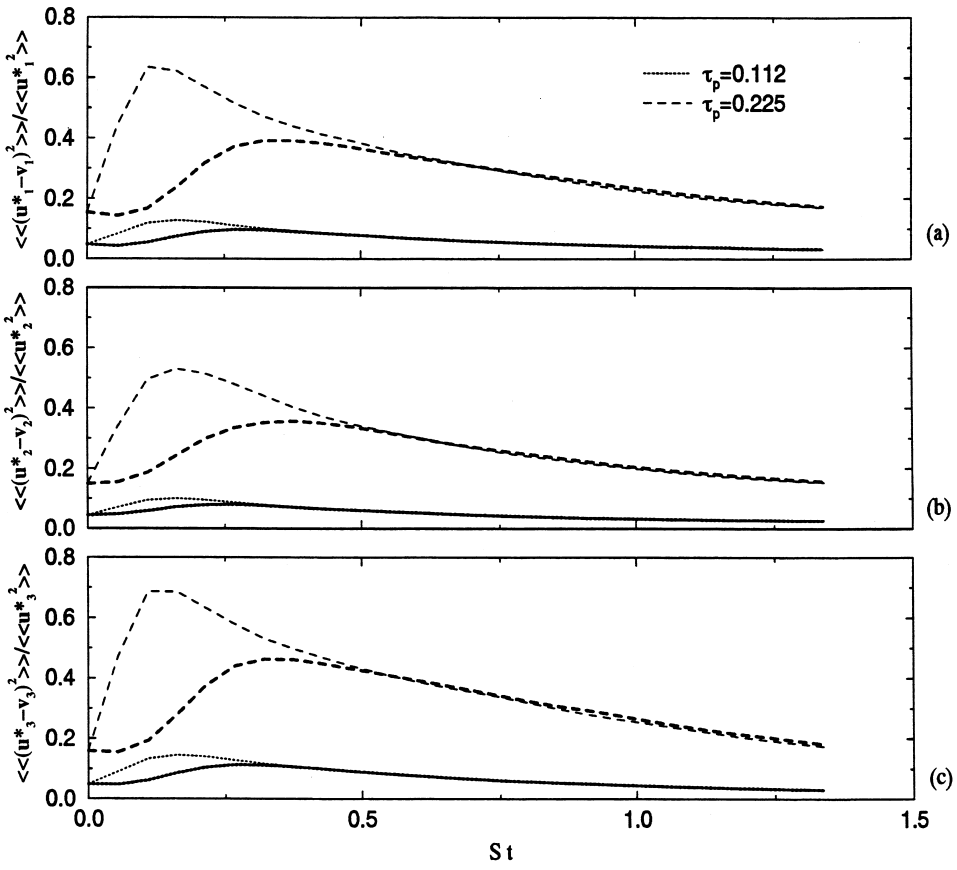

Fig. 9. Comparison of the mean-square relative fluctuating velocity for different initial conditions for the particle mean velocity; (a) in the elongated direction x_1, (b) in the shortened direction x_2, (c) in the spanwise direction x_3. Thick lines for $V_{2,2}(0) = -S$ and thin lines for $V_{2,2}(0) = \xi_2$.

for $\tau_p < \tau_{p_{cr}}$, and

$$\frac{\ll \left(u_2^* - v_2\right)^2 \gg}{\ll \left(u_2^*\right)^2 \gg} \geq \frac{\ll \left(u_3^* - v_3\right)^2 \gg}{\ll \left(u_3^*\right)^2 \gg}, \tag{5.5}$$

for $\tau_p > \tau_{p_{cr}}$.

Although it is not certain that the particles are independent of their initial conditions once the mean-square relative velocity has reached a maximum value, the occurrence of the peak time does provide an indication that the particles are no longer significantly influenced by their initial conditions. Fig. 9 compares the present results (thick lines) for the evolution of mean-square relative velocity of smaller particles ($\tau_p = 0.112$ and 0.225) with the results (thin lines) from similar simulations, but initialized as $V_{2,2}\ (t = 0) = \xi_2$ which is the asymptotic value of $V_{2,2}$. We observe that although t_{peak} has decreased with this new initial condition, after some initial time the curves merge and the values of $\ll (u_i^* - v_i)^2 \gg / \ll (u_i^*)^2 \gg$ are almost independent of the initializations. This is particularly important for model assessments as most turbulence closures are based on the assumption of dynamic equilibrium.

We now consider both the homogeneous and inhomogeneous dispersed phases. The effect of particle inertia is examined through trajectory plots, and quantified dispersion results are given by calculating the particles mean-square displacement. In Fig. 10, trajectories are plotted by

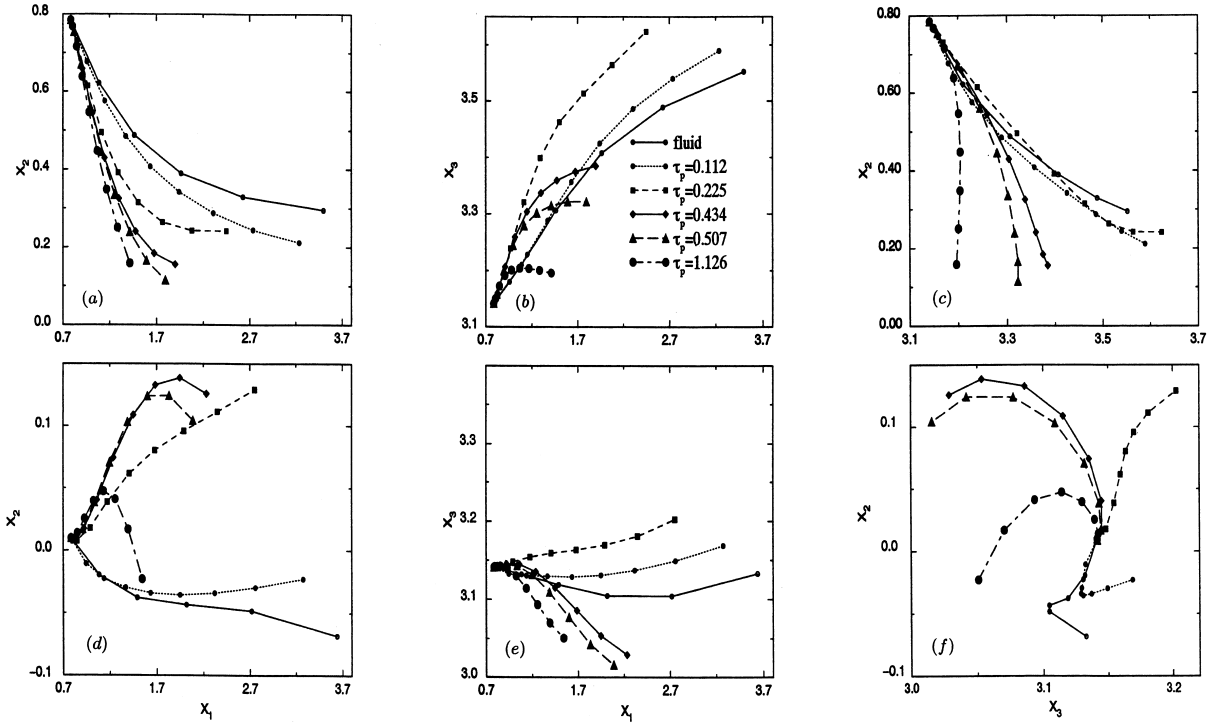

Fig. 10. Projection onto the $(x_1, x_2), (x_1, x_3)$, and (x_2, x_3) planes of the trajectories of the tracer fluid and solid particles for various particle time constants; (a)–(c) Injection Location 1, (d)–(f) Injection Location 2.

tracking the instantaneous positions of a single particle as it moves through the flow. Trajectory plots can be used to analyze various means for particle dispersion such as centrifugal and inertial mechanisms. The plots also show the particles accelerations and decelerations in the flow field and the effect of increased drag on larger particles. For the trajectory results presented, particle time constants ranging from 0.112 to 1.126 are used, with the injection mean velocity calculated from the mean velocity gradients indicated in Tables 1–3 (the initial fluctuating velocity is taken equal to that of the local fluid). For comparison, the trajectory of the fluid particle is also provided. Injection was simulated for two different locations: Location 1 ($X_1^{\text{inj}} = \pi/4$, $X_2^{\text{inj}} = \pi/4$, $X_3^{\text{inj}} = \pi$) and Location 2 ($X_1^{\text{inj}} = \pi/4$, $X_2^{\text{inj}} = 0.01$, $X_3^{\text{inj}} = \pi$).

Fig. 10 shows the trajectories projected onto the (x_1, x_2), (x_1, x_3), and (x_3, x_2)-planes. As indicated in the figure, the particles are strongly influenced by their inertia and injection location. In general, small particles ($\tau_p/\tau_k = 0.5$) follow the fluid particles relatively closely, whereas the large particles ($\tau_p/\tau_k > 1.5$) remain almost unaffected by the turbulence and their motion seems to be dominated by their mean velocity. For heavy particles injected from Location 2, an oscillatory behavior in x_2-direction can be observed in Fig. 10(d,f) for $\tau_p > \tau_{p_{cr}}$. For this injection location, the dispersion in x_1-direction is consistent with the mean velocities — the mean velocity for heavy particles decreases with τ_p in x_1-direction and for a non-zero X_1^{inj} the dispersion is mostly due to the mean motion. In Fig. 10(d,f), we see that the fluid and small solid particles cross the x_1-axis, whereas the heavy particles initially tend to move upwards, before being directed back to the x_1-axis for $\tau_p > \tau_{p_{cr}}$. Notice that the heavy particles have a lower initial momentum due to the low injection velocity assumed in x_2-direction, $\hat{V}_2(0) = v_2 - SX_2^{\text{inj}} \simeq v_2$, and the smaller mean velocity in x_1-direction. Therefore, this behavior of the heavier particles may be associated to the increased drag on them coupled with their initially imparted low momentum. The medium-size particles ($\tau_p/\tau_k = 1$) exhibit an interesting behavior. Their trajectory, although very different from that of the fluid particles, is strongly influenced by the fluid turbulence. In fact, depending upon the injection location, they can be dispersed more than the fluid particles. This is the case for particles with $\tau_p = 0.225$, injected close to the (x_1, x_3)-plane, that is at $X_1^{\text{inj}} = \pi/4$ and $X_2^{\text{inj}} = 0.01$ (Fig. 10d–f).

In order to quantify the dispersion of the particles, the dispersion function (or r.m.s. displacement) of a solid or fluid particle in the x_α-direction is calculated from:

$$D_{\alpha\alpha}(t) = \left[\frac{1}{N}\sum_{i=1}^{N}\left(\hat{X}_\alpha^{(i)}(t) - X_\alpha^{\text{inj}}\right)^2\right]^{\frac{1}{2}} \tag{5.6}$$

where N is the total number of particles in the flow field at time t, $\hat{X}_\alpha^{(i)}$ is the instantaneous position of particle (i) at time t, and X_α^{inj} is the injection location of the same particle. Fig. 11 shows the variation of the dispersion function with time for various particle time constants for an injection location close to the x_3-axis ($X_1^{\text{inj}} = 0.01$, $X_2^{\text{inj}} = 0.01$, $X_3^{\text{inj}} = \pi$). The dispersion function generally increases with time since the particles disperse increasingly farther from their injection location. At earlier times, the dispersion seems to be the highest for $\tau_p = 0.112$, whereas at longer times the fluid particles exhibit the highest amount of dispersion. It is observed that for long times the dispersion in x_1 and x_3 directions decreases significantly as

the inertia increases. The reason is that, as the turbulence fluctuations grow in time, it becomes more difficult for larger particles to follow the turbulent motions. This is similar to the results found by Yeh and Lei (1991) in the case of homogeneous turbulent shear flows.

To further investigate the effects of the particle inertia and the injection location on dispersion, in Fig. 12 the value of the dispersion function at the final time, $St = 1.38$, is plotted

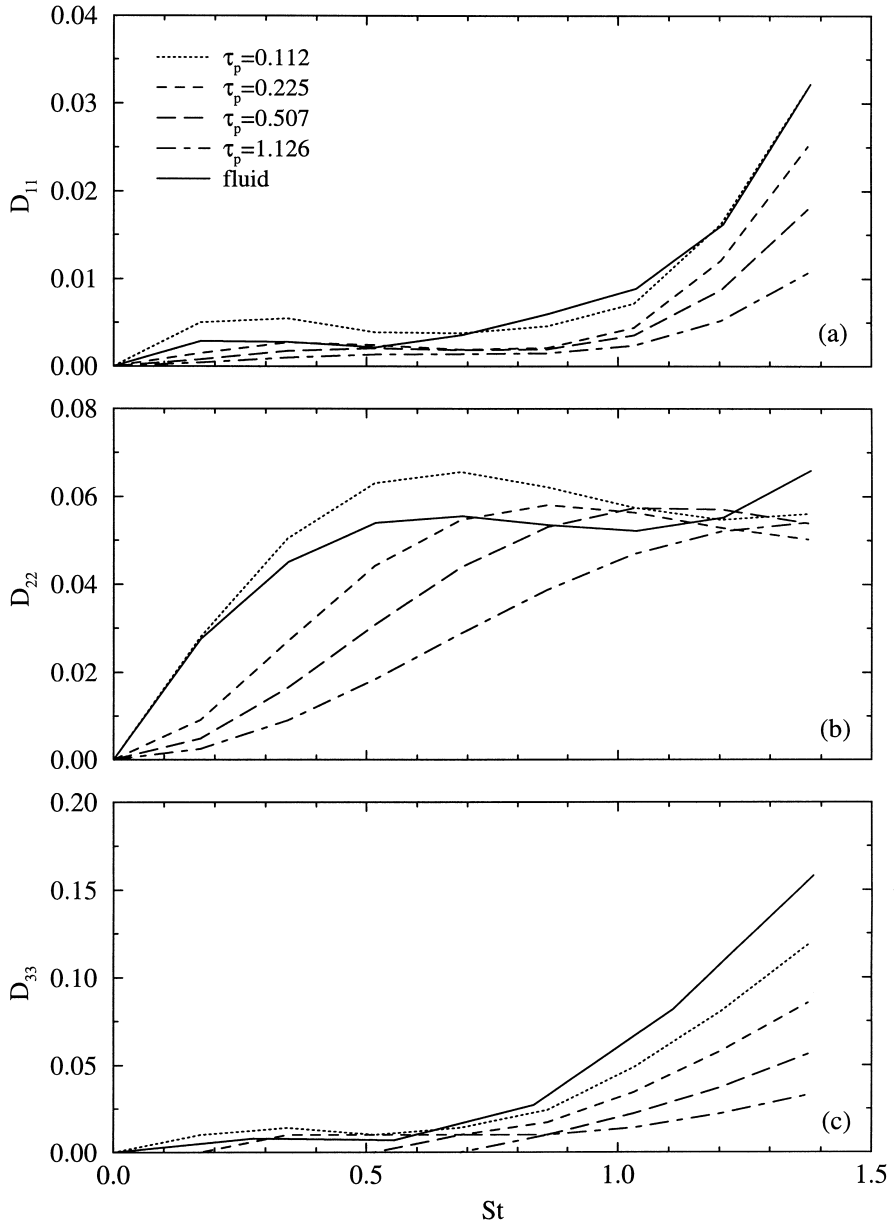

Fig. 11. Dispersion function for fluid and solid particles for different particle time constants; particles injected at $X_1^{\text{inj}} = 0.01$, $X_2^{\text{inj}} = 0.01$, and $X_3^{\text{inj}} = \pi$.

versus the particle time constant, normalized with the Kolmogorov time scale, for various injection locations. For all of the cases shown in Fig. 12, $X_3^{\text{inj}} = \pi$. It is noted that in x_1-direction, the dispersion always decreases with the increase of the particle time constant, and is larger for $X_1^{\text{inj}} = \pi/4$ than for $X_1^{\text{inj}} = 0.01$, which is a direct result of the larger magnitudes of the instantaneous velocity of the particles with $X_1^{\text{inj}} = \pi/4$ in the x_1-direction. The same trend

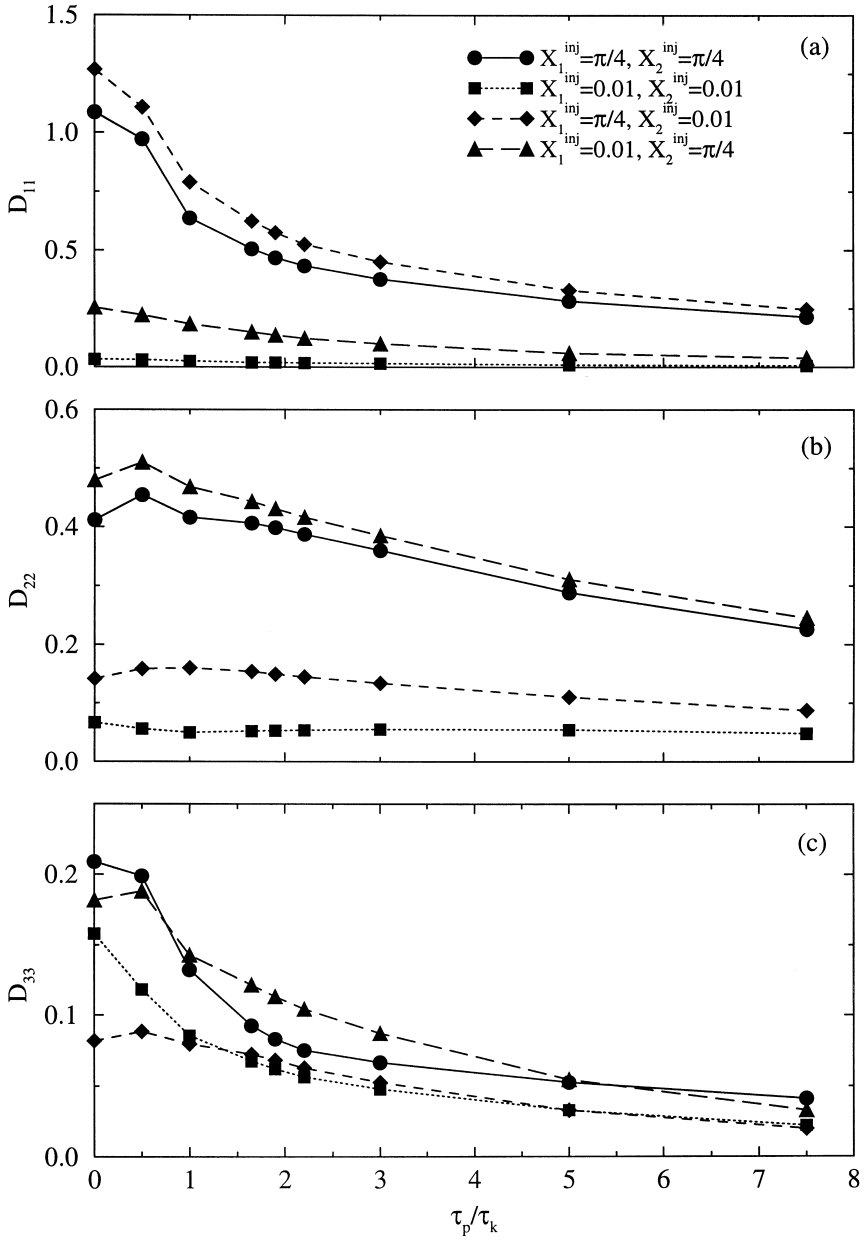

Fig. 12. Effect of injection location on dispersion for various particle time constants.

is observed in x_2-direction, that is, the particles disperse more at larger values of X_2^{inj}. However, it is observed that, for particles injected away from x_3-axis, dispersion in x_2-direction is enhanced for small particle time constant, i.e. $\tau_p/\tau_k = 0.5$. Fig. 12a also shows an interesting feature pertaining to the influence of large mean velocity in opposite directions. We see that for small X_1^{inj}, D_{11} is increased by a larger X_2^{inj} (i.e. a larger initial velocity in x_2-direction), whereas for large X_1^{inj} an increase in $V_2(t=0)$ results in a decrease in D_{11}. A similar behavior is observed in Fig. 12b for D_{22} when X_1^{inj} is varied for a constant X_2^{inj}. The variation of the dispersion in x_3-direction is somewhat irregular. A decrese in D_{33} is observed with the increase of particle inertia but it is noted that for injection locations $(X_1^{\text{inj}},\ X_2^{\text{inj}}) = (\pi/4,\ 0.01)$ and $(0.01,\ \pi/4)$ the solid particles with $\tau_p/\tau_k = 0.5$ disperse more than the fluid particles. The effect of the mean motion in increasing particle dispersion in the spanwise direction is clearly observed by comparing the dispersion for the injection locations $(X_1^{\text{inj}} = X_2^{\text{inj}} = \pi/4)$ and $(X_1^{\text{inj}} = X_2^{\text{inj}} = 0.01)$, the former being always larger than the latter. Notice that, it is difficult to describe a general trend for the influence of the mean motion on D_{33}.

The important observations pertaining to particle dispersion are that the particles mean square displacement generally increases with time and that it is a decreasing function of particle inertia for most cases. If we limit the comparison to the cases with $X_1^{\text{inj}} = X_2^{\text{inj}} = \pi/4$ and $X_1^{\text{inj}} = X_2^{\text{inj}} = 0.01$, it can be concluded that an increase in the particles mean velocity increases the particle dispersion function, including the dispersion in x_3-direction which represents the 'turbulent' dispersion only. For the dispersion in x_1- and x_2-directions, it is observed that an increase in X_1^{inj} (X_2^{inj}) results in an increase in D_{11} (D_{22}).

6. Summary and concluding remarks

Results obtained by direct numerical simulation (DNS) are used to investigate particle-laden homogeneous plane strain turbulent flows. An analysis of the averaged equations of motion for the dispersed phase indicates that there is always a relative mean velocity between the particle and its surrounding fluid. Under the assumption of small particle Reynolds number, the dispersed phase is shown to be homogeneous and an analytical solution is found for the particle mean velocity. This allows the calculation of the statistics involving the particle fluctuating velocity for cases with small particle time constant. The analytical solution for the mean velocity of small particles also shows the existence of a critical particle time constant beyond which the particles follow an oscillatory trajectory about the elongated (x_1) axis. For large particles, the empirical correction added to the drag coefficient prevents a homogeneous solution for the dispersed phase. The results generated for large particles are mainly used to study the dispersion characteristics of the particles.

In the case of homogeneous dispersed phase, the DNS results show that the particle velocity autocorrelation increases with the increase of the particle time constant in all directions during the initial times. For longer dispersion times the reverse is observed as the particles are subjected to the crossing-trajectories effect caused by the difference in the mean velocities of the two phases. The particle turbulence kinetic energy increases with the increase of the particle time constant at early times when the turbulence is decaying. An opposite trend is observed in the stage of turbulence growth. The dispersed phase shows a stronger anisotropy than the

carrier phase, with the level of anisotropy increasing with the increase of the particle time constant. It is observed that the r.m.s. of the particle fluctuating velocity in the shortened direction increases over that of the fluid. Also, this r.m.s. velocity component increases with the increase of the particle time constant which is the opposite to the trend previously observed in isotropic turbulence but is similar to the theoretical and DNS results for the streamwise component in turbulent shear flows.

For both homogeneous and inhomogeneous dispersed phases, the trajectories of individual particles injected from different locations indicate that the small inertia particles closely follow the fluid particles, whereas particles with larger time constants are not significantly influenced by the turbulence. Particles with time constants of the order of the Kolmogorov time scale (when not over-influenced by their mean velocity) exhibit trajectories which are very different from those of the fluid particles. A quantified dispersion study indicates that the light particles disperse more than the high inertia particles, and usually less than the fluid particles, in all three directions. A large injection velocity seems to increase the particles dispersion. In the strained directions, increasing the injection location component X_i^{inj} produces a larger dispersion in the respective x_i-direction.

Altough it has not been attempted in this work, the results and the analysis presented here can be helpful for future model development and assessment. Due to the presence of a mean relative velocity between the two phases, plane strain particle-laden flows offer several unique features which are not feasible via DNS of other flows such as isotropic or homogeneous shear. These include, the crossing-trajectories (and its accompanying continuity) effects (Fig. 4) and the compressibility of the dispersed phase (Fig. 2). This is while the homogeniety of the plane strain flow has allowed us to calculate accurate statistics involving the velocity fluctuations of the dispersed phase. This feature distinguishes the flow from inhomogeneous channel flow which has been extensively utilized for DNS of particle-laden flows. Our previous experience in implementing DNS results for validation of both statistical (Mashayek et al., 1998) and stochastic (Mashayek, 1999) models indicate that the ability to capture the above features of particle-laden flows play a significant role in the success of turbulence models and must be addressed via comparisons in simple flows for which accurate data are available.

Acknowledgements

F. Mashayek acknowledges the support of the National Science Foundation and the Office of Naval Research under Grants CTS-9874655 and N00014-99-1-0808, respectively. Computational resources were provided by the San Diego Supercomputing Center.

Appendix A

In this appendix we show that $\ll v_j \frac{\partial v_i}{\partial x_j} \gg = 0$ for a homogeneous dispersed phase. Consider the change of coordinates: $\alpha_i = -x_i$. The new velocity fields are:

$$\hat{\Gamma}_i = -\hat{U}_i, \quad \hat{\Lambda}_i = -\hat{V}_i. \tag{A.1}$$

Defining Γ_i the (fluid) average of $\hat{\Gamma}_i$, Λ_i the (particle) average of $\hat{\Lambda}_i$, $\gamma_i = \hat{\Gamma}_i - \Gamma_i$, and $\lambda_i = \hat{\Lambda}_i - \Lambda_i$, we have:

$$\Gamma_{i,j} = \frac{\partial \Gamma_i}{\partial \alpha_j} = \frac{\partial U_i}{\partial x_j} = U_{i,j}, \quad \Lambda_{i,j} = \frac{\partial \Lambda_i}{\partial \alpha_j} = \frac{\partial V_i}{\partial x_j} = V_{i,j}. \tag{A.2}$$

The mean velocity gradient tensors are the same in the two coordinate systems and thus, the statistics of the turbulence will be the same. In particular,

$$\ll v_j \frac{\partial v_i}{\partial x_j} \gg = \ll \lambda_j \frac{\partial \lambda_i}{\partial \alpha_j} \gg . \tag{A.3}$$

However, since $\hat{\Lambda}_i = -\hat{V}_i$ we also have:

$$\ll v_j \frac{\partial v_i}{\partial x_j} \gg = - \ll \lambda_j \frac{\partial \lambda_i}{\partial \alpha_j} \gg . \tag{A.4}$$

From (A.3) and (A.4) we conclude:

$$\ll v_j \frac{\partial v_i}{\partial x_j} \gg = 0. \tag{A.5}$$

Appendix B

The mean velocity of the dispersed phase can be determined from the solution for x_i. The initial conditions are such that $V_\alpha(0) = \sigma_\alpha^0(0) x_\alpha(0)$. Since $\xi_1 \neq \eta_1$, we can assume either $\sigma_1^0 \neq \xi_1$ or $\sigma_1^0 \neq \eta_1$. If $\sigma_1^0 \neq \xi_1$, then:

$$V_1 = \frac{\eta_1 \exp(\eta_1 t) + \dfrac{\sigma_1^0 - \eta_1}{\xi_1 - \sigma_1^0} \xi_1 \exp(\xi_1 t)}{\exp(\eta_1 t) + \dfrac{\sigma_1^0 - \eta_1}{\xi_1 - \sigma_1^0} \exp(\xi_1 t)} x_1, \tag{B.1}$$

otherwise:

$$V_1 = \xi_1 x_1. \tag{B.2}$$

Similarly, if $\tau_p < \tau_{p_{cr}}$ and $\sigma_2^0 \neq \xi_2$:

$$V_2 = \frac{\eta_2 \exp(\eta_2 t) + \dfrac{\sigma_2^0 - \eta_2}{\xi_2 - \sigma_2^0} \xi_2 \exp(\xi_2 t)}{\exp(\eta_2 t) + \dfrac{\sigma_2^0 - \eta_2}{\xi_2 - \sigma_2^0} \exp(\xi_2 t)} x_2, \tag{B.3}$$

and for $\sigma_2^0 = \xi_2$:

$$V_2 = \xi_2 x_2. \tag{B.4}$$

If $\tau_p = \tau_{p_{cr}}$:

$$V_2 = \frac{\sigma_2^0 - \left(\sigma_2^0 + \dfrac{1}{2\tau_p}\right)\dfrac{t}{2\tau_p}}{1 + \left(\sigma_2^0 + \dfrac{1}{2\tau_p}\right)t} x_2. \tag{B.5}$$

When $\tau_p > \tau_{p_{cr}}$ we obtain:

$$V_2 = \frac{\sigma_2^0 + \dfrac{-1}{2\tau_p\omega}\left(\sigma_2^0 + 2S\right)\tan(\omega t)}{\sigma_2^0 + \dfrac{1}{2\tau_p}} x_2. \tag{B.6}$$
$$1 + \frac{\sigma_2^0 + \dfrac{1}{2\tau_p}}{\omega}\tan(\omega t)$$

For the x_3-direction, if $\sigma_3^0 \neq 0$:

$$V_3 = \frac{\exp\left(\dfrac{-t}{\tau_p}\right)}{\dfrac{1 + \tau_p\sigma_3^0}{\sigma_3^0} - \tau_p\exp\left(\dfrac{-t}{\tau_p}\right)} x_3, \tag{B.7}$$

otherwise:

$$V_3 = 0. \tag{B.8}$$

References

Barré, C., 1998. Direct numerical simulation of particle-laden plane strain turbulent flows. M.S. Thesis, Department of Mechanical and Aerospace Engineering, State University of New York at Buffalo, Buffalo, NY.

Blaisdell, G.A., Mansour, N.N., Reynolds, W.C., 1991. Numerical simulation of compressible homogeneous turbulence. Department of Mechanical Engineering Report TF-50, Stanford University, Stanford, CA.

Brooke, J.W., Hanratty, T.J., McLaughlin, J.B., 1994. Free-flight mixing and deposition of aerosols. Phys. Fluids 6, 3404–3415.

Crowe, C.T., Troutt, T.R., Chung, J.N., 1996. Numerical models for two-phase turbulent flows. Ann. Rev. Fluid Mech. 28, 11–43.

Csanady, G.T., 1963. Turbulent diffusion of heavy particles in the atmosphere. J. Atmos. Sci. 20, 201–208.

Faeth, G.M., 1987. Mixing, transport and combustion in sprays. Prog. Energy Combust. Sci. 13, 293–345.

Jackson, R., 1997. Locally averaged equations of motion for a mixture of identical spherical particles and a Newtonian fluid. Chem. Eng. Sci. 52, 2457–2469.

Kwak, D., Reynolds, W.C., Ferziger, J.H., 1975. Three dimensional time dependent computation of turbulent flows. Stanford University Report TF-5, Department of Mechanical Engineering, Stanford University, Stanford, CA.

Lee, M.J., Reynolds, W.C., 1985. Numerical experiments on the structure of homogeneous turbulence. Department of Mechanical Engineering Report TF-24, Stanford University, Stanford, CA.

Liljegren, L.M., 1993. The effect of a mean fluid velocity gradient on the streamwise velocity variance of a particle suspended in a turbulent flow. Int. J. Multiphase Flow 19, 471–484.
Ling, W., Chung, J.N., Troutt, T.R., Crowe, C.T., 1998. Direct numerical simulation of a three-dimensional temperature mixing layer with particle dispersion. J. Fluid Mech. 358, 61–85.
Mashayek, F., Jaberi, F.A., Miller, R.S., Givi, P., 1997. Dispersion and polydispersity of droplets in stationary isotropic turbulence. Int. J. Multiphase Flow 23, 337–355.
Mashayek, F., Taulbee, D.B., Givi, P., 1998. Modeling and simulation of two-phase turbulent flow. In: Roy, G.D. (Ed.), Propulsion Combustion: Fuels to Emissions. Taylor and Francis, Washington, DC, pp. 241–280 (chapter 8).
Mashayek, F., 1998. Droplet-turbulence interactions in low-Mach-number homogeneous shear two-phase flows. J. Fluid Mech. 376, 163–203.
Mashayek, F., 1999. Stochastic simulations of particle-laden isotropic turbulent flow. Int. J. Multiphase Flow 25, 1575–1599.
Maxey, M.R., 1987. The gravitational settling of aerosol particles in homogeneous turbulence and random flow fields. J. Fluid Mech. 174, 441–465.
McLaughlin, J.B., 1989. Aerosol particle deposition in numerically simulated channel flow. Phys. Fluids 1, 1211–1224.
Miller, R.S., Bellan, J., 1999. Direct numerical simulation of a confined three-dimensional gas mixing layer with one evaporating hydrocarbon-droplet laden stream. J. Fluid Mech. 384, 293–338.
Pan, Y., Banerjee, S., 1996. Numerical simulation of particle interactions with wall turbulence. Phys. Fluids 8, 2733–2755.
Reeks, W.M., 1993. On the constitutive relations for dispersed particles in nonuniform flows. Part I: Dispersion in a simple shear flow. Phys. Fluids 5, 750–761.
Riley, J.J., Patterson, G.S., 1974. Diffusion experiments with numerically integrated isotropic turbulence. Phys. Fluids 17, 292–297.
Rogallo, R.S., Moin, P., 1984. Numerical simulation of turbulent flow. Ann. Rev. Fluid Mech. 16, 99–137.
Simonin, O., Deutsch, E., Boivin, M., 1995. Large eddy simulation and second-moment closure model of particle fluctuating motion in two-phase turbulent shear flows. In: Durst, F., Kasagi, N., Launder, B.E., Schmidt, F.W., Whitelaw, J.H. (Eds.), Turbulent Shear Flows 9. Springer–Verlag, Berlin, pp. 85–115.
Taulbee, D.B., Mashayek, F., Barré, C., 1999. Simulation and Reynolds stress modeling of particle-laden turbulent shear flows. Int. J. Heat Fluid Flow 20, 368–373.
Tucker, H.J., Reynolds, A.J., 1968. The distortion of turbulence by irrotational plane strain. J. Fluid Mech. 32, 657–673.
Wallis, G.B., 1969. One Dimensional Two Phase Flow. McGraw-Hill, New York.
Wang, L-P., Maxey, M.R., 1993. Settling velocity and concentration distribution of heavy particles in isotropic turbulence. J. Fluid Mech. 256, 27–68.
Wen, F., Kamalu, N., Chung, J.N., Crowe, C.T., Troutt, T.R., 1992. Particle dispersion by vortex structures in plane mixing layers. J. Fluids Eng. 114, 657–666.
Yeh, F., Lei, U., 1991. On the motion of small particles in a homogeneous turbulent shear flow. Phys. Fluids 3, 2758–2776.
Yudine, M.I., 1959. Physical considerations on heavy-particle diffusion. Adv. Geophys. 6, 185–191.
Zhang, D.Z., Prosperetti, A., 1997. Momentum and energy equations for disperse two-phase flows and their closure for dilute suspensions. Int. J. Multiphase Flow 23, 425–453.
Zhou, L.X., 1993. Theory and Numerical Modeling of Turbulent Gas-Particle Flows and Combustion. CRC Press, Boca Raton, FL.